

Quarterly Report for
January - March 2001
Stanford Geothermal Program
DE-FG07-99ID13763

Table of Contents

1. MEASUREMENTS OF STEAM-WATER RELATIVE PERMEABILITY	1
1.1 BACKGROUND	1
1.2 EXPERIMENTAL PROCEDURE	1
1.3 EXPERIMENTAL RESULTS	2
1.4 FUTURE RESEARCH	3
2. STEAM-WATER RELATIVE PERMEABILITY BY THE CAPILLARY PRESSURE METHOD	4
2.1 SUMMARY	4
2.2 INTRODUCTION	4
2.3 THEORY	5
2.4 RESULTS	8
2.5 DISCUSSION	13
2.6 CONCLUSIONS	14
2.7 FUTURE WORK	14
3. WETTABILITY IN STEAM-WATER-ROCK SYSTEMS	15
3.1 SUMMARY	15
3.2 INTRODUCTION	15
3.3 MATHEMATICS	15
3.4 EXPERIMENTS	18
3.5 RESULTS	18
3.6 CONCLUSIONS	22
3.7 FUTURE WORK	23
4. FRACTURED ROCK RELATIVE PERMEABILITY	24
4.1 BACKGROUND	24
4.2 EXPERIMENTAL METHODOLOGY	24

4.3 PARTIAL RESULTS AND DISCUSSION	26
4.4 CONTINUING AND FUTURE WORK	29
5. MEASUREMENT OF CAPILLARY PRESSURE IN GEOTHERMAL ROCKS	31
5.1 BACKGROUND	31
5.2 PRELIMINARY EXPERIMENTS	32
5.3 NEW EXPERIMENT	33
5.4 PARTIAL RESULT AND DISCUSSION	35
5.5 ELECTRICAL RESISTIVITY TOMOGRAPHY EXPERIMENT	36
5.6 FUTURE WORK	38
6. EXPERIMENTAL INVESTIGATION OF STEAM AND WATER RELATIVE PERMEABILITY ON SMOOTH WALLED FRACTURE	39
6.1 BACKGROUND	39
6.2 EXPERIMENTAL APPARATUS AND MEASUREMENT TECHNIQUES	40
6.3 PARTIAL RESULTS AND DISCUSSION	43
6.5 USE OF NEW APPARATUS FOR NITROGEN WATER EXPERIMENTS	49
6.4 FUTURE WORK	51
7. REFERENCES	52

1. MEASUREMENTS OF STEAM-WATER RELATIVE PERMEABILITY

This research project is being conducted by Research Assistant Peter O'Connor and Professor Roland Horne. The aim is to measure relative permeability relations for steam and water flowing simultaneously in rock and to examine the effects of temperature.

1.1 BACKGROUND

An X-ray CT technique has been used in recent years to measure the distribution of steam and water saturation in rocks to obtain steam-water relative permeability curves (Satik and Horne, 1998, Mahiya, 1999).

The current experiment maintains a constant pressure, to eliminate possible effects of temperature on relative permeability. As the experiment is constantly at an inlet pressure of 15 psig, it will necessarily be at a constant 120°C at the inlet in order to have two-phase flow throughout, with the rest of the core being at the saturation temperature for the pressure at that point. The experiment has maintained an identical pressure profile and temperature profile for most flow tests. These results can then be used as a baseline for future experiments at a different temperature and pressure gradient.

1.2 EXPERIMENTAL PROCEDURE

The Berea sandstone core was drained, flushed with nitrogen, then subjected to a vacuum. A dry X-ray scan was then made to obtain CT_{dry} . The core was saturated with water and scanned to obtain CT_{wet} ; from these scans, a porosity distribution was obtained. In the next step, hot liquid water was flowed through to obtain CT_{hw} , which is necessary to calculate experimental saturations. Flow-through experiments were then conducted at a pressure gradient of approximately 15 psi across the 41-cm length. First, the core was saturated with steam. Steam flow rate was gradually lowered to implement an imbibition process whereby the wetting phase (water) displaces the nonwetting phase (steam). A flexible heat guard ensured negligible overall heat loss for a near-adiabatic process. The flexible heat guard control mechanism was redesigned last year. At each step, the system reached a steady state and was subjected to a CT scan to measure saturation. Steam flow rate was reduced to 0%, then increased. In the drainage sequence, steam displaced water. This sequence produced more readings at high water saturation, with less certainty of the actual mobile saturation.

At each stage, pressure, temperature and heat fluxes from the core were measured. Calculated relative permeability to steam and water remain to be plotted against the saturation measurements. The major change from the previous experiment was to perform the imbibition step first. Performing the imbibition step first allows determination of the maximum pressure and power input. This pressure can be maintained by increasing flow rates if necessary.

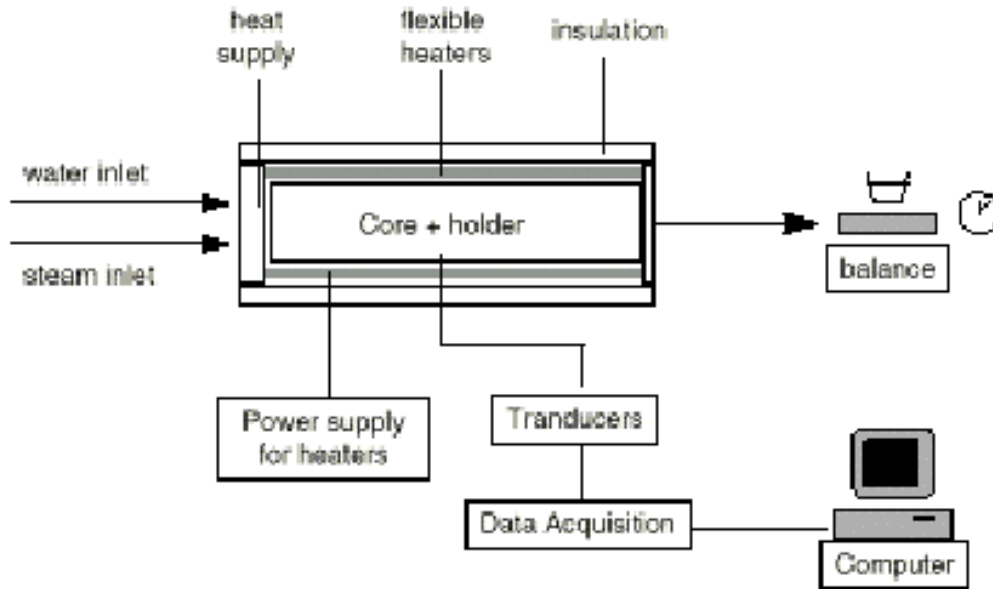


Figure 1.1: Experimental apparatus for relative permeability measurement.

1.3 EXPERIMENTAL RESULTS

During the quarter, we completed all the flow tests and CT scans. The complete data set remains to be analyzed, though some results are currently available. Flow tests completed included 14 imbibition tests, spanning the full range of saturations, and 14 drainage tests, predominantly focusing on high and moderate water saturation. Failure of the inlet pumps necessitated resorting to two-phase flow from a single inlet for some drainage tests. These tests will be evaluated as estimated results using total saturation from the CT scans and established relations between total saturation and mobile saturation, and the results from these steps will be distinguished from all other results. The steel end piece presented some challenges that the previous plastic one did not; there appears to be greater heat flow between the fluid heaters. As a result, we do not have absolute confidence in single-phase flow from each inlet, though the CT scans should provide some insight in this regard. Future experiments should consider an alternate design of the endpiece.

The resulting pressure/temperature gradients showed great uniformity in most cases of two-phase flow, as illustrated by Figure 1.2. Analyzed data so far has focused on tests conducted at high steam saturation. These results have shown a Corey-type curve for steam-water relative permeability, as shown in Figure 1.3, though water relative permeability has in some cases been less than expected. Preliminary analysis of the high water saturation tests appears to show a maximum water relative permeability of around

0.57 (not included in Figure 1.3), though additional analysis is required. A harmonic average of the relative permeabilities taken at different points along the core appears to provide a reasonable method to mitigate anomalies caused by equipment calibration. These averages will be presented in the final report, along with the complete data and data specific to a few of the most reliable instruments.

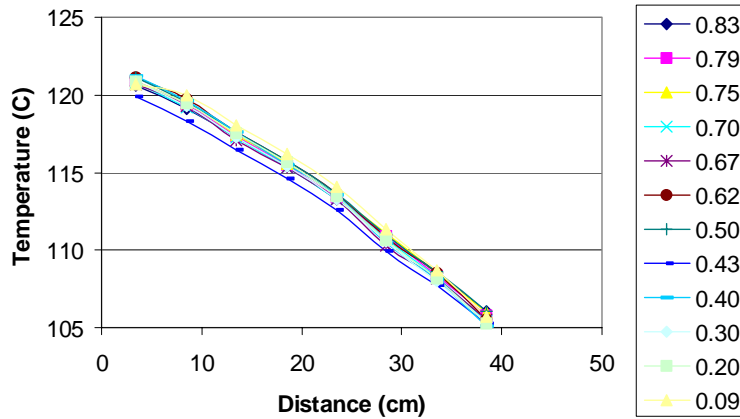


Figure 1.2: Temperature profiles for 12 two-phase flow imbibition tests.

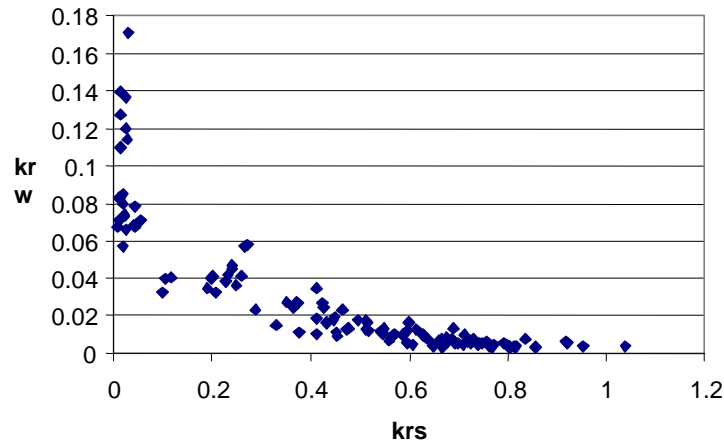


Figure 1.3: Steam relative permeability vs water relative permeability (estimated); uncorrected for slip factor.

1.4 FUTURE RESEARCH

Future research may involve repeating the experiment at different pressure gradients and temperatures. The next experiment will probably occur at approximately half the current pressure gradient. In each case, the experiment will maintain a uniform pressure gradient for the range of saturations. The current apparatus is not likely to be suitable for conducting a similar experiment at significantly higher pressure gradients or temperature. Several suggestions are being prepared for apparatus modifications for future experiments.

2. STEAM-WATER RELATIVE PERMEABILITY BY THE CAPILLARY PRESSURE METHOD

This research project is being conducted by Research Associate Kewen Li and Professor Roland Horne. The objective is to develop a method to calculate steam-water relative permeability by using data from steam-water capillary pressure measurements.

2.1 SUMMARY

In this work, various capillary pressure techniques such as the Purcell, Burdine, Corey and Brooks-Corey methods were used to calculate steam-water relative permeabilities from the measured steam-water capillary pressure data in both drainage and imbibition processes. The calculated results were compared to experimental data of steam-water relative permeability measured directly. The steam-water relative permeability and capillary pressure were measured simultaneously. The differences between the Purcell model and the measured values were almost negligible for water phase relative permeability but not for the steam phase. The effect of tortuosity factor on the wetting phase was revealed to be insignificant in this case. The values of steam phase relative permeability calculated by other models were very close to the experimental values for drainage but very different for imbibition as expected. The same calculation was made for the nitrogen-water flow to confirm the observation in the steam-water flow. The results showed that it would be possible and useful to calculate steam-water relative permeability using the capillary pressure method, especially for the drainage case.

2.2 INTRODUCTION

Steam-water relative permeability plays an important role in controlling reservoir performance for steam injection into oil reservoirs and water injection into geothermal reservoirs. However, it is difficult to measure steam-water relative permeability because of the phase transformation and the significant mass transfer between the two phases as pressure changes. On the other hand, Li and Horne (2001b) found significant differences between steam-water and air-water capillary pressures, and Horne *et al.* (2000) found significant differences between steam-water and air-water relative permeabilities. Therefore, steam-water flow properties may not be simply replaced by air (or nitrogen)-water flow properties. It would be helpful for reservoir engineers to be able to calculate steam-water relative permeability once steam-water capillary pressure is available.

There are a number of papers related to the capillary pressure method for the calculation of oil-gas relative permeabilities. Honarpour *et al.* (1986) reviewed the literature in this field. The published literature and experimental data for relative permeability and capillary pressure were not sufficient to conclude which method should be the standard one.

Unlike for oil-gas flow properties, there are few studies for the calculation of steam-water relative permeabilities by the capillary pressure technique. Historically, the capillary pressure techniques were developed for drainage situations and were useful to obtain gas-liquid (oil or water) relative permeability when fluid flow tests were not practical. As stated previously, it is difficult to measure steam-water relative permeability. Therefore,

we calculated the steam-water relative permeability in this study using data from measurements of steam-water capillary pressure in both drainage and imbibition experiments. The steam-water capillary pressures were measured at a temperature of about 120°C in a Berea sandstone sample. The steam-water relative permeabilities were computed by different capillary pressure techniques and compared to the measured data in the same core sample using a steady-state method in which the fluid saturation was measured with an X-ray CT scanner.

2.3 THEORY

We chose four representative models developed by various authors to calculate steam-water relative permeabilities from capillary pressure measurements. The mathematical expressions of the four models are described in this section.

Purcell Model

Purcell (1949) developed an equation to compute rock permeability by using capillary pressure data. This equation can be extended to the calculation of multiphase relative permeability. In two-phase flow, the relative permeability of the wetting phase can be calculated as follows:

$$k_{rw} = \frac{\int_0^{S_w} dS_w / (P_c)^2}{\int_0^1 dS_w / (P_c)^2} \quad (2.1)$$

where k_{rw} and S_w are the relative permeability and saturation of the wetting phase; P_c is the capillary pressure as a function of S_w .

Similarly, the relative permeability of the nonwetting phase can be calculated as follows:

$$k_{rnw} = \frac{\int_{S_w}^1 dS_w / (P_c)^2}{\int_0^1 dS_w / (P_c)^2} \quad (2.2)$$

where k_{rnw} is the relative permeability of the nonwetting phase. It can be seen from Eqs. 2.1 and 2.2 that the sum of the wetting and nonwetting phase relative permeability at a specific saturation is equal to one. This may not be true in most porous media. In the next section, the relative permeabilities calculated using this method are compared to the experimental data. The comparison shows that Eq. 2.1 is close to experimental values of the wetting phase relative permeability but Eq. 2.2 is far from the experimental results.

Burdine Model

Burdine (1953) developed equations similar to Purcell's method by introducing a tortuosity factor as a function of wetting phase saturation. The relative permeability of the wetting phase can be computed as follows:

$$k_{rw} = (\lambda_{rw})^2 \frac{\int_0^{S_w} dS_w / (P_c)^2}{\int_0^1 dS_w / (P_c)^2} \quad (2.3)$$

where λ_{rw} is the tortuosity ratio of the wetting phase. According to Burdine (1953), λ_{rw} could be calculated as follows:

$$\lambda_{rw} = \frac{\tau_w(1.0)}{\tau_w(S_w)} = \frac{S_w - S_m}{1 - S_m} \quad (2.4)$$

where S_m is the minimum wetting phase saturation from the capillary pressure curve; $\tau_w(1.0)$ and $\tau_w(S_w)$ are the tortuosities of the wetting phase when the wetting phase saturation is equal to 100% and S_w respectively.

In the same way, relative permeabilities of the nonwetting phase can be calculated by introducing a nonwetting phase tortuosity ratio. The equation can be expressed as follows:

$$k_{rnw} = (\lambda_{rnw})^2 \frac{\int_{S_w}^1 dS_w / (P_c)^2}{\int_0^1 dS_w / (P_c)^2} \quad (2.5)$$

where k_{rnw} is the relative permeability of the nonwetting phase; λ_{rnw} is the tortuosity ratio of the nonwetting phase, which can be calculated as follows:

$$\lambda_{rnw} = \frac{\tau_{nw}(1.0)}{\tau_{nw}(S_w)} = \frac{1 - S_w - S_e}{1 - S_m - S_e} \quad (2.6)$$

here S_e is the equilibrium saturation of the nonwetting phase; τ_{nw} is the tortuosity of the nonwetting phase.

Honarpour *et al.* (1986) pointed out that the expression for the wetting phase relative permeability (Eq. 2.3) fits the experimental data much better than the expression for the nonwetting phase (Eq. 2.5).

Corey Model

According to the Purcel and Burdine models, an analytical expression for the wetting and nonwetting phase relative permeabilities may be obtained if capillary pressure curves can be represented by a simple mathematical function. Corey (1954) found that oil-gas capillary pressure curves could be expressed approximately using the following linear relation:

$$1/P_c^2 = CS_w^* \quad (2.7)$$

where C is a constant and S_w^* is the normalized wetting phase saturation expressed as follows:

$$S_w^* = \frac{S_w - S_{wr}}{1 - S_{wr}} \quad (2.8a)$$

where S_{wr} is the residual saturation of the wetting phase or water phase in steam-water flow. In Corey's case, S_{wr} is the residual oil saturation.

Although the Corey model was not originally developed for the imbibition case, in this study it was used to calculate the imbibition steam-water relative permeabilities by defining the normalized wetting phase saturation as follows:

$$S_w^* = \frac{S_w - S_{wr}}{1 - S_{wr} - S_{nwr}} \quad (2.8b)$$

where S_{nwr} is the residual saturation of the nonwetting phase, representing the residual steam saturation in this study.

Substituting Eq. 2.7 into Eqs. 3 and 5 with the assumption that $S_e=0$ and $S_m=S_{wr}$, Corey (1954) obtained the following equations to calculate the wetting (oil) and nonwetting (gas) phase relative permeabilities for drainage cases:

$$k_{rw} = (S_w^*)^4 \quad (2.9)$$

$$k_{rmw} = (1 - S_w^*)^2 [1 - (S_w^*)^2] \quad (2.10)$$

A constraint to the use of Corey's model (Eqs. 2.9 and 2.10) is that the capillary pressure curve can be represented by Eq. 2.7.

Brooks-Corey Model

Because of the limitation of Corey's Model, Brooks and Corey (1966) modified the representation of capillary pressure function to a more general form as follows:

$$P_c = p_e (S_w^*)^{-1/\lambda} \quad (2.11)$$

where p_e is the entry capillary pressure and λ is the pore size distribution index.

Substituting Eq. 2.11 into the Burdine model (Eqs. 2.3 and 2.5) with the assumption that $S_e=0$, Brooks and Corey (1966) derived equations to calculate the wetting and nonwetting phase relative permeabilities as follows:

$$k_{rw} = (S_w^*)^{\frac{2+3\lambda}{\lambda}} \quad (2.12a)$$

$$k_{rnw} = (1 - S_w^*)^2 \left[1 - (S_w^*)^{\frac{2+\lambda}{\lambda}} \right] \quad (2.12b)$$

When λ is equal to 2, the Brooks-Corey Model is reduced to the Corey Model.

2.4 RESULTS

The data of both drainage and imbibition steam-water capillary pressure from Li and Horne (2001a) were used to calculate the corresponding steam-water relative permeability. Note that the capillary pressure data were represented using Eq. 2.11 in all the calculations by the Purcell model. The calculated results were compared to the experimental data of steam-water relative permeability (Mahiya, 1999). During the process of the fluid flooding tests, the water saturation in the core sample was first decreased from 100% to the remaining water saturation, about 28%, representing a drainage process. The water saturation was then increased, representing an imbibition. The calculations and the comparisons are presented in this section.

Fig. 2.1 shows the experimental data of the steam-water relative permeability and capillary pressure in drainage. All these data were measured at a temperature of about 120°C in the same Berea core sample. Because the relative permeability and the capillary pressure were measured simultaneously, the two curves had the same residual water saturations. This feature is important and will be discussed in more detail later. Note that the steam relative permeability data shown in Fig. 2.1 have been calibrated under the consideration of gas slippage in two-phase flow by Li and Horne (2001a).

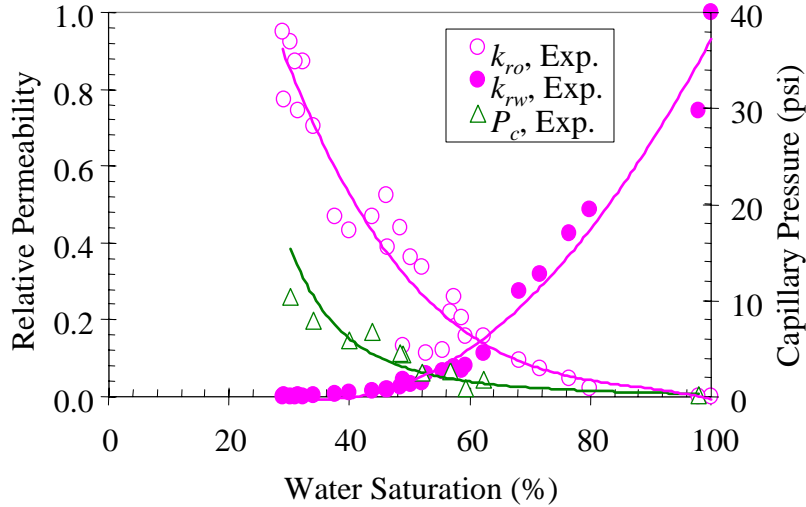


Figure 2.1: Experimental data of drainage steam-water relative permeability and capillary pressure (Mahiya, 1999; Li and Horne, 2000).

The drainage steam-water relative permeabilities were calculated using the data of the drainage steam-water capillary pressure shown in Fig. 2.1 and plotted versus the normalized water saturation that is defined in Eq. 2.8a. The calculated results and the comparison to the corresponding experimental data are shown in Fig. 2.2. The water relative permeabilities calculated using the Purcell model are the best fit to the experimental data. This implies that it may not be necessary to adjust the calculation of the wetting phase relative permeabilities by introducing the concept of the tortuosity factor in such a case. The water phase relative permeabilities calculated by all the other models are less than the experimental values. It can be seen from Fig. 2.2 that the steam phase (nonwetting phase) relative permeabilities calculated by all the models but the Purcell model are almost the same and consistent with the experimental data for the drainage case. The steam phase relative permeabilities calculated by the Purcell model are not shown in Fig. 2.2 and all the figures following in this section because the curve is concave to the axis of the normalized water saturation on the Cartesian plot, which is unexpected and far from the experimental values.

The experimental data of the imbibition steam-water relative permeability and the imbibition capillary pressure are shown in Fig. 2.3. These data were also measured simultaneously in the same Berea core sample at a temperature of about 120°C. The steam relative permeability data shown in Fig. 2.3 have been calibrated under the consideration of gas slippage in two-phase flow.

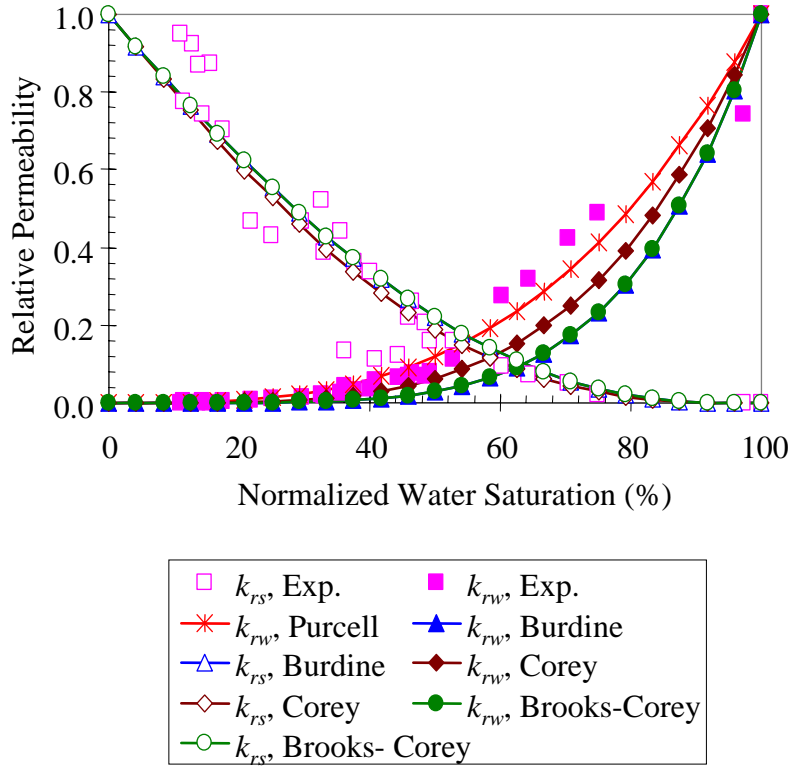


Figure 2.2: Calculated steam-water relative permeability and the comparison to the experimental data in drainage case.

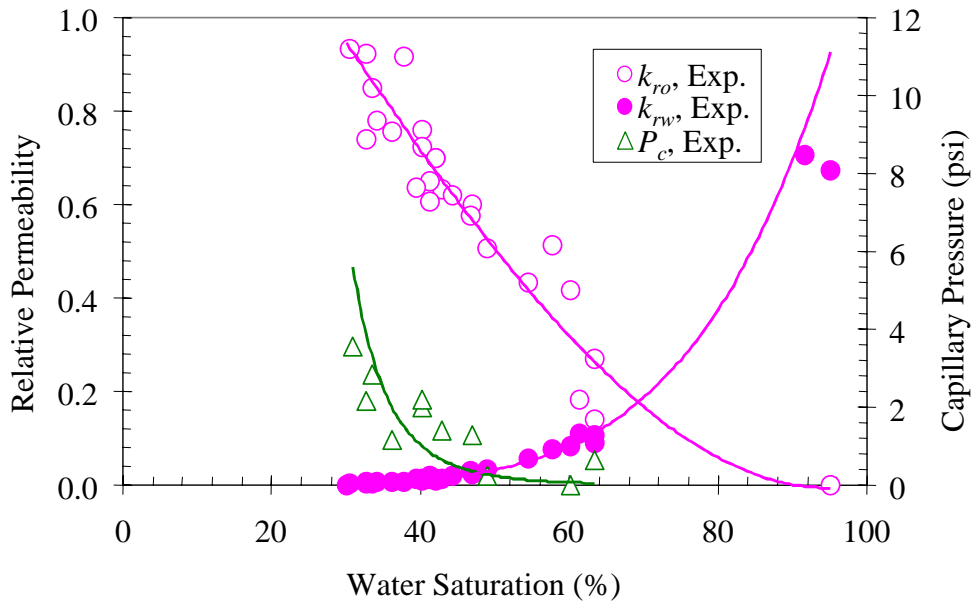


Figure 2.3: Experimental data of imbibition steam-water relative permeability and capillary pressure (Mahiya, 1999; Li and Horne, 2000).

The imbibition steam-water relative permeabilities were then calculated using the measured data of the imbibition steam-water capillary pressure shown in Fig. 2.3 and also plotted versus the normalized water saturation. Fig. 2.4 shows the calculated results and the comparison to the experimental values. The water relative permeabilities from the Purcell model are still the best fit to the experimental data. The results from the Corey model are a good fit too. The water phase relative permeabilities calculated by the Burdine and the Brooks-Corey models are less than the experimental values. Actually the results calculated using the two models are the same if the capillary pressure data in the Burdine model are represented using Eq. 2.11. The steam phase relative permeabilities calculated by all the models except the Purcell Model are not significantly different from each other but are much less than the experimental data for the imbibition case.

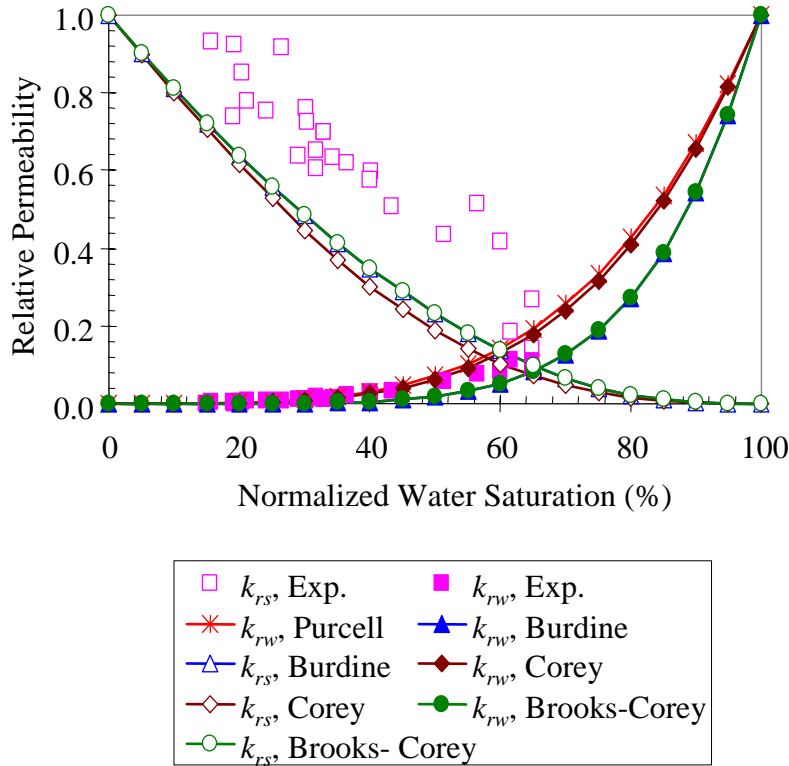


Figure 2.4: Calculated steam-water relative permeability and the comparison to the experimental data in imbibition case.

In the following section, we will discuss the calculated results and the comparison in nitrogen-water systems. Li and Horne (2001a) measured the nitrogen-water relative permeabilities in a Berea core sample similar to that used in the measurement of steam-water relative permeabilities by Mahiya (1999). In this study, we drilled a plug from another part of the same Berea sandstone that was used by Li and Horne (2001a). The length and diameter of the plug sample were 5.029 cm and 2.559 cm respectively; the porosity was 24.37%. The drainage nitrogen-water capillary pressure of the plug was measured by using the semipermeable porous-plate method. The measured data of the drainage nitrogen-water capillary pressure along with the relative permeabilities by Li

and Horne (2001a) are plotted in Fig. 2.5. Although the capillary pressure and relative permeability curves were not measured simultaneously, the residual water saturations were the same for both.

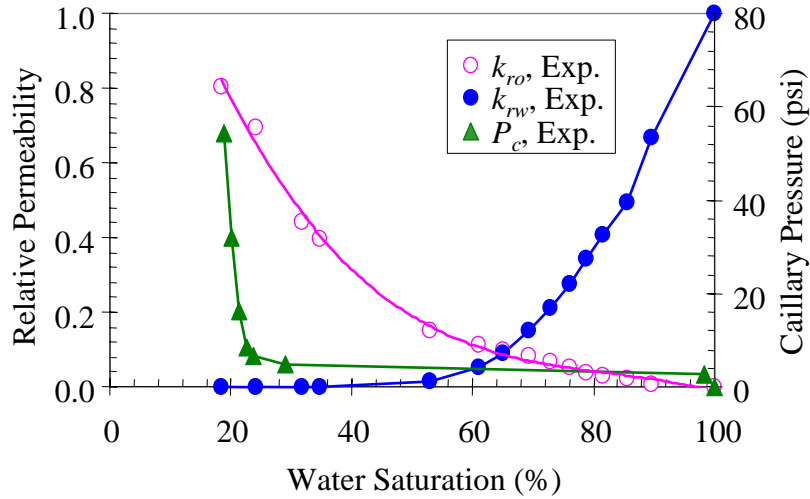


Figure 2.5: Experimental data of drainage nitrogen-water relative permeability and capillary pressure.

The results calculated using the capillary pressure models for the nitrogen-water flow (drainage) and the comparison to the experimental data are shown in Fig. 2.6. The experimental data of water relative permeability are located between the Purcell model and the Corey model. The two models provide a good approximation to the experimental data in this case. The features of gas phase relative permeability curve calculated by these models are similar to those of steam-water flow (see Fig. 2.4) except that the calculated results are greater than the measured data.

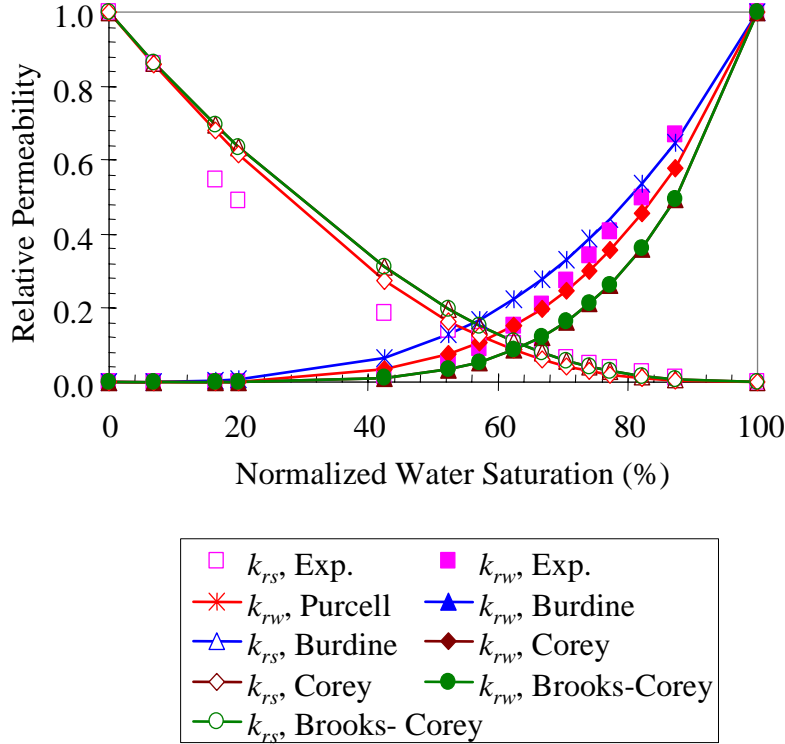


Figure 2.6: Calculated nitrogen-water relative permeability and the comparison to the experimental data in drainage.

We made the same calculation and comparison using the data of oil-water relative permeability and capillary pressure measured by Kleppe and Morse (1974). We also observed that the best fit to the wetting phase relative permeability was from the Purcell model. However, we did not observe the same phenomenon for the data by Gates and Leitz (1950). In summarizing all the calculations that we have made, the Purcell model was the best fit to the wetting phase relative permeability if the measured capillary pressure curve had the same residual wetting saturation as the relative permeability curve.

2.5 DISCUSSION

The technique of using capillary pressure to calculate relative permeability was developed in the late forties but has not been widely utilized. Burdine (1953) pointed out that the calculated relative permeabilities are more consistent and probably contain less maximum error than the measured data because the error in measurement is unknown. This may be true in some cases. However, the differences between different capillary pressure models are obvious, especially for the wetting phase. Therefore, one of the questions is which model is most appropriate for practical use. The calculations in this study showed that the Purcell model was the best fit to the wetting phase relative permeability. This seems surprising because the concept of the tortuosity factor as a function of wetting phase saturation is not necessarily introduced for the calculation of the wetting phase relative permeability in such a case. Burdine (1953) obtained an empirical expression for the effective tortuosity factor as a function of wetting phase

saturation (see Eq. 2.4). λ_{rw} is actually the ratio of the tortuosity at 100% wetting phase saturation to the tortuosity at a wetting phase saturation of S_w . The tortuosity of wetting phase is infinite at the minimum wetting phase saturation according to Eq. 2.4. This may not be true because the wetting phase may exist on the rock surface in the form of continuous film. In this case, $\tau_w(S_m)$ may be close to $\tau_w(1.0)$, which demonstrates the insignificant effect of the wetting phase saturation on the tortuosity of the wetting phase. Similarly, based on Eq. 2.6, the tortuosity of the nonwetting phase is infinite when the wetting phase saturation is equal to $1-S_e$. This may be true because the nonwetting phase may exist in the form of discontinuous droplets. It can be seen from the analysis here that the tortuosity of wetting and nonwetting phases would behave differently as a function of wetting phase saturation. This may be why it is necessary to introduce the tortuosity for the nonwetting phase but not for the wetting phase.

2.6 CONCLUSIONS

Based on the present work, the following conclusions may be drawn:

1. In steam-water flow, the calculated results indicate that the Purcell model may be the best fit to the experimental data of the water phase relative permeability for both drainage and imbibition processes but is not a good fit for the steam phase.
2. The Corey model could also provide a good approximation to the measured data of the wetting phase relative permeability in some cases.
3. Except for the Purcell model, the results of the steam phase relative permeability calculated using the models for the drainage case were almost the same and very close to the experimental values. However, those for the imbibition case were smaller than the measured data.
4. The consistency between the residual wetting saturations of capillary pressure curve and relative permeability curve is important to the comparison of modeling results with the measured data.
5. Because of the difficulty of measuring steam-water relative permeability, the capillary pressure technique may be very useful for practical application.

2.7 FUTURE WORK

We plan to calculate relative permeability with the capillary pressure technique by collecting more experimental data.

3. WETTABILITY IN STEAM-WATER-ROCK SYSTEMS

This research project was conducted by Research Associate Kewen Li and Professor Roland Horne. The goal of this study is to develop a method to determine the wettability in steam-water-rock systems.

3.1 SUMMARY

In this study we developed a method to infer the wettability index or the contact angle in steam-water-rock systems from the experimental data of steam-water capillary pressure and relative permeability. The method was based on the relationship between permeability and capillary pressure developed by Purcell (1949). The values of the wettability index in steam-water-rock systems were calculated for both drainage and imbibition processes. The results demonstrated that the value of the wettability index in the drainage case was greater than that in the imbibition case. This implies that the corresponding contact angle in the drainage case is smaller than that in the imbibition case, which is reasonable.

3.2 INTRODUCTION

Gas-liquid-rock systems are usually considered to be strongly liquid-wet, which is true in most natural fluid-rock systems. It is also usually assumed that the contact angle through the liquid phase is zero in gas-liquid-rock systems, which may not be true. The values of the wettability index in different gas-liquid-rock systems may not be the same. Li and Horne (2001a) found significant differences between steam-water and air-water capillary pressures, and Horne *et al.* (2000) found significant differences between steam-water and air-water relative permeabilities. We therefore speculated that there might be differences of wettability between steam-water-rock and air-water-rock systems. Unfortunately, there are few methods to evaluate the wettability in gas-liquid-rock systems.

Purcell (1949) developed a model to correlate the rock permeability and the pore size distribution that could be inferred from capillary pressure curves. According to this relationship, we developed a method to calculate the wettability index or contact angle in steam-water-rock systems from the data of steam-water capillary pressure. This method was also extended to two-phase flow to verify whether the wettability is a function of fluid saturation. In this case, both capillary pressure and relative permeability data are required to calculate the wettability index at different fluid saturation. The values of the wettability index in both drainage and imbibition processes were calculated and compared.

3.3 MATHEMATICS

Using Poiseuille's equation and Darcy's Law, Purcell (1949) derived a relationship between the rock permeability and the capillary pressure curve as follows:

$$k = F\phi(\sigma \cos \theta)^2 \int_0^1 \frac{dS_w}{P_c^2} \quad (3.1)$$

where k and ϕ are the absolute permeability and porosity of the rock; F is the so-called lithology factor. σ and θ are the interfacial tension between the two fluids and the contact angle through the liquid phase; P_c and S_w are the capillary pressure and the saturation of the wetting phase.

Brooks and Corey (1966) suggested a function to represent capillary pressure curves as follows:

$$P_c = p_e (S_w^*)^{-1/\lambda} \quad (3.2)$$

where p_e is the entry capillary pressure and λ is the pore size distribution index; S_w^* is the normalized wetting phase saturation. For drainage case, it is expressed as follows:

$$S_w^* = \frac{S_w - S_{wr}}{1 - S_{wr}} \quad (3.3)$$

where S_{wr} is the residual saturation of the wetting phase or water phase in steam-water flow.

Although the capillary pressure function suggested by Brooks and Corey (1966) was not originally for imbibition cases, in this study it was used to calculate the wettability index in the imbibition case by defining the normalized wetting phase saturation as follows:

$$S_w^* = \frac{S_w - S_{wr}}{1 - S_{wr} - S_{nwr}} \quad (3.4)$$

where S_{nwr} is the residual saturation of the nonwetting phase, representing the residual steam saturation in this study.

Substituting Eq. 3.2 into Eq. 3.1:

$$k = F\phi \left(\frac{\sigma \cos \theta}{P_e} \right)^2 \frac{\lambda}{\lambda + 2} \quad (3.5)$$

The wettability index was defined as $\cos \theta$, According to Eq. 3.5, it can be calculated as follows:

$$W_i = \cos \theta = \sqrt{\left(\frac{\lambda + 2}{\lambda} \right) \left(\frac{k}{F\phi} \right) \frac{P_e}{\sigma}} \quad (3.6)$$

where W_i is the wettability index. The only unknown parameter in Eq. 3.6 is the lithology factor, F once the capillary pressure curve is available. The values of the lithology factor were determined by Purcell (1949) for numerous rock samples by means of comparing the air permeability to the permeability calculated using Eq. 3.1. The capillary pressure curves were measured by the technique of mercury injection. The values of the lithology factor obtained by Purcell (1949) ranged from 0.08 to 0.36. The lithology factor was found to be smaller in lower permeability rock.

The contact angle through the liquid phase can be also calculated from Eq. 3.6 once the capillary pressure curve and the lithology factor are known. Note that the contact angle calculated in such a way may be different from that defined in a capillary tube or on a flat solid surface in concept. Actually, this value represents the macroscopic average contact angle of the fluid-rock system.

Assuming that Eq. 3.1 applies in two-phase flow, it is written as follows:

$$k_w = F\phi(\sigma \cos \theta_w)^2 \int_0^{S_w} \frac{dS_w}{P_c^2} \quad (3.7)$$

where k_w and θ_w are the effective permeability of the wetting phase and the contact angle through the wetting phase. Because F is a parameter representing lithology, it is assumed in this study that it does not vary with the saturation of the wetting phase.

Substituting Eq. 3.2 into Eq. 3.7, the following equation can be obtained:

$$W_{iw} = \cos \theta_w = \sqrt{\left(\frac{\lambda + 2}{\lambda}\right) \left(\frac{k_w}{FS_w^* \phi}\right) \frac{P_c}{\sigma}} \quad (3.8)$$

where W_{iw} is the wettability index at the wetting phase saturation of S_w . Eq. 3.8 can also be expressed as follows:

$$W_{iw} = \cos \theta_w = \sqrt{\left(\frac{\lambda + 2}{\lambda}\right) \left(\frac{k}{F\phi}\right) \left(\frac{k_{rw}}{S_w^*}\right) \frac{P_c}{\sigma}} \quad (3.9)$$

where k_{rw} is the relative permeability of the wetting phase. It can be seen from Eq. 3.9 that if the wettability of a fluid-rock system does not change with the fluid saturation, as

it is usually assumed, then $\sqrt{\left(\frac{k_{rw}}{S_w^*}\right) P_c}$ should be constant. This may be verified by using

the data from the simultaneous measurements of capillary pressure and relative permeability curves.

Another important significance of Eq. 3.9 is that it may be possible to determine the wettability of steam-water-rock systems by using the data from a simple spontaneous water imbibition experiment. Because the relative permeability and the capillary pressure

at a specific water saturation can be calculated simultaneously from spontaneous water imbibition tests according to the method developed by Li and Horne (2000a), the wettability index can be obtained from Eq. 3.9. Therefore, we can obtain the wettability information without measuring the whole capillary pressure curve. λ can be deduced by using two different fluid pairs such as air-water and steam-water to conduct the measurements.

3.4 EXPERIMENTS

The measured data of the steam-water capillary pressure from Li and Horne (2000b) and the relative permeability from Mahiya (1999) were used in this study. The experimental apparatus, test procedures, and the properties of the rock and fluid samples were reported by Mahiya (1999) and Li and Horne (2000b).

3.5 RESULTS

Few reliable data of capillary pressure and relative permeability measured simultaneously are available in the literature. To verify the method we developed in this study, the data from Kleppe (1974) were used to calculate the wettability index at different fluid saturations. The imbibition oil-water capillary pressure data from Kleppe (1974) are shown in Fig. 3.1 on a log-log plot in order to obtain the value of λ . These data were measured in a Berea sandstone sample by water injection. The oil phase was kerosene.

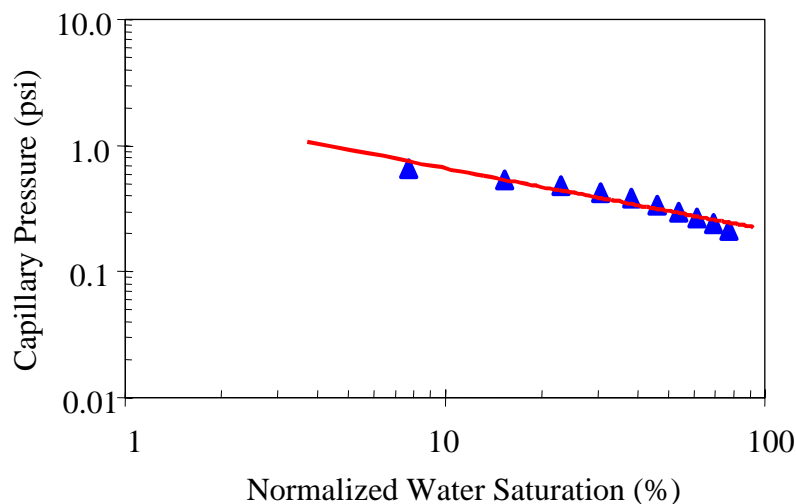


Figure 3.1: Capillary pressure data from Kleppe (1974).

Using Eq. 3.2 to represent the capillary pressure curve in Fig. 3.1, the value of λ we obtained was about 2.06. Because the value of the lithology factor is unknown for this rock sample, both the minimum and maximum values determined by Purcell (1949) were utilized in the calculation. As stated previously, the value of the lithology factor determined by Purcell (1949) ranged from 0.08 to 0.36 for rock samples with permeabilities ranging from 3 to 1500 md. The permeability of the rock sample used by Kleppe (1974) was about 290 md which was within this range. The wettability index and

the corresponding contact angle were calculated using Eq. 3.6 and the results are listed in Table 3.1.

Table 3.1: Results of Wettability Index and Contact Angle for Different Values of F.

F (Lithology Factor)	W_i (Wettability Index)	θ (Contact Angle)
0.08	0.12	83.1
0.36	0.06	86.8

The calculated results in Table 3.1 demonstrate that the effect of the lithology factor on the contact angle is not very significant in this case. Therefore the minimum value, 0.08, of the lithology factor determined by Purcell (1949) was used in the rest of the calculations in this study. Note that the effect of the lithology factor on the contact angle may be significant at some specific values of the wettability index.

It can also be seen from Table 3.1 that the oil-water-rock (Berea sandstone) is water-wet, which is consistent with the actual wettability. The significance of the value of the wettability index in Table 3.1 may not be exactly the same as those of the wettability index obtained by the Amott and the USBM methods. However, it is certain that the closer the value of the wettability index to 1.0, the stronger the wettability of the liquid phase through which the contact angle is measured.

Even though it is usually assumed that the wettability does not vary with water saturation, there are few experimental data available to verify the assumption due to the scarcity of methods to evaluate the wettability at a specific water saturation. For this purpose, the values of the wettability index and the corresponding contact angle at different water saturation were calculated using Eq. 3.9 with the measured data of the oil-water capillary pressure and the relative permeability from Kleppe (1974). The calculated results are plotted in Fig. 3.2.

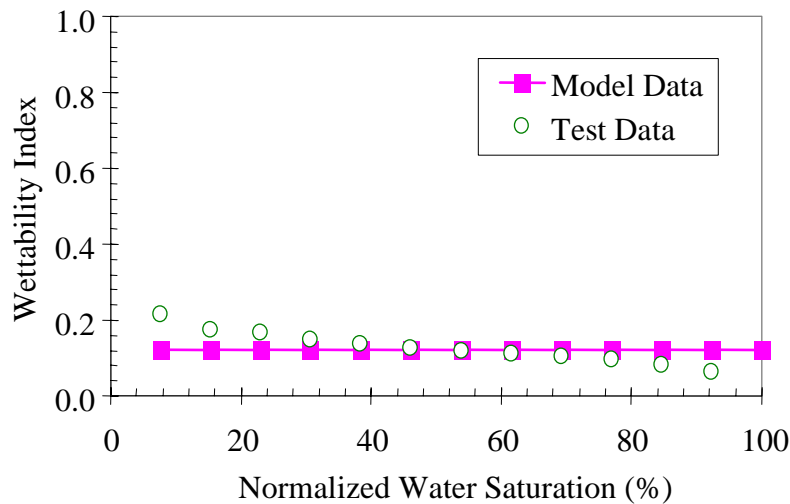


Figure 3.2: Wettability index calculated using data from Kleppe (1974).

The model data of the wettability index shown in Fig. 3.2 were calculated using the data of the capillary pressure and the relative permeability from modeling. In this study, the modeling capillary pressure data were calculated using Eq. 3.2 and the modeling relative permeability data were computed using the Purcell model which is expressed as follows:

$$k_{rw} = (S_w^*)^{\frac{2+\lambda}{\lambda}} \quad (3.10)$$

The reason we used the Purcell model was that Li and Horne (2001b) found it to provide the best fit to the wetting phase relative permeability, as described earlier in Section 2 of this report.

It can be seen from Fig. 3.2 that the wettability index does not vary significantly with the water saturation and is very close to the model data. The wettability index calculated using the modeling capillary pressure and relative permeability data is equal to that calculated using Eq. 3.6 (only capillary pressure data were used). The calculated results of the corresponding contact angle are shown in Fig. 3.3. Accordingly, the contact angle calculated using Eq. 3.9 at different water saturation is almost constant and close to the model results. This implies that we may be able to determine the wettability index or the contact angle using the relative permeability and the capillary pressure at only one point of specific water saturation instead of over the whole range of the curve.

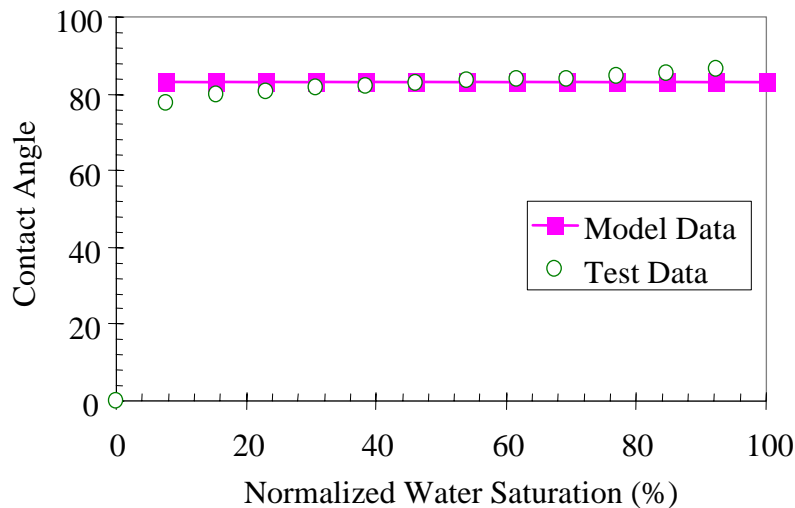


Figure 3.3: Contact angle calculated using data from Kleppe (1974).

Now we will discuss the calculations of the wettability index in steam-water-rock systems. The steam-water capillary pressure curves from Li and Horne (2000b) were utilized. Both the drainage and the imbibition capillary pressure curves from Li and Horne (2000b) are plotted in Fig. 3.4 in log-log coordinates to obtain the values of λ for the calculations using Eq. 3.6 or Eq. 3.9. These data were measured in a fired Berea

sandstone sample at a temperature of about 120°C using a steady-state flow method. The values of λ for the drainage and the imbibition cases are 0.543 and 0.715 respectively.

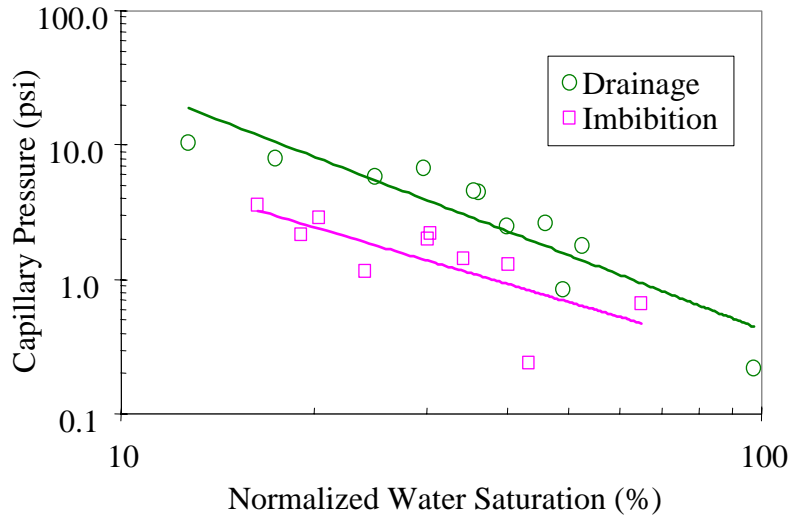


Figure 3.4: Capillary pressure data from Li and Horne (2000b).

Fig. 3.5 shows the values of the wettability index calculated with the model data of the steam-water capillary pressure and relative permeability representing the experimental data from Li and Horne (2000b). The results calculated directly using the measured data are not plotted in Fig. 3.5 because several values of the wettability index are much greater than 1.0, which is unexpected. The reason may be due to the scatter in the steam-water capillary pressure data.

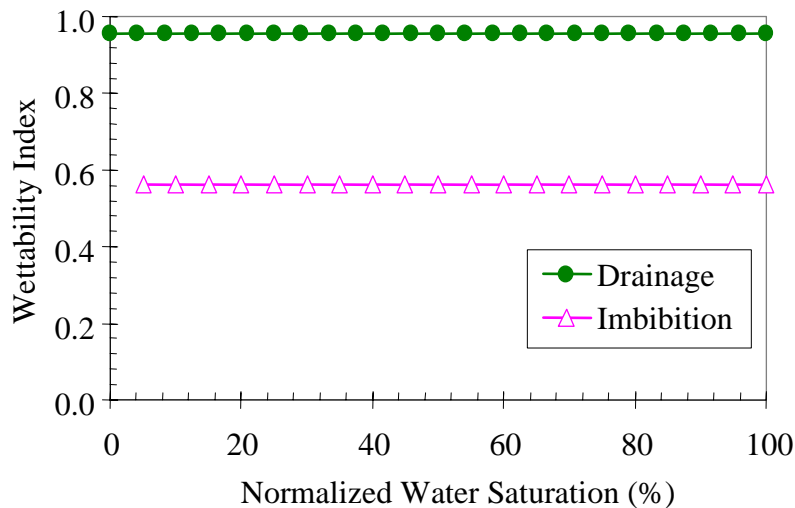


Figure 3.5: Wettability index calculated using data from Li and Horne (2000b).

We can see from Fig. 3.5 that the wettability index in the imbibition case is less than that in the drainage case, which is theoretically correct and has been proven experimentally by

Morrow and McCaffery (1978). The values of the corresponding contact angle were calculated using the wettability index data from Fig. 3.5 and the results are shown in Fig. 3.6.

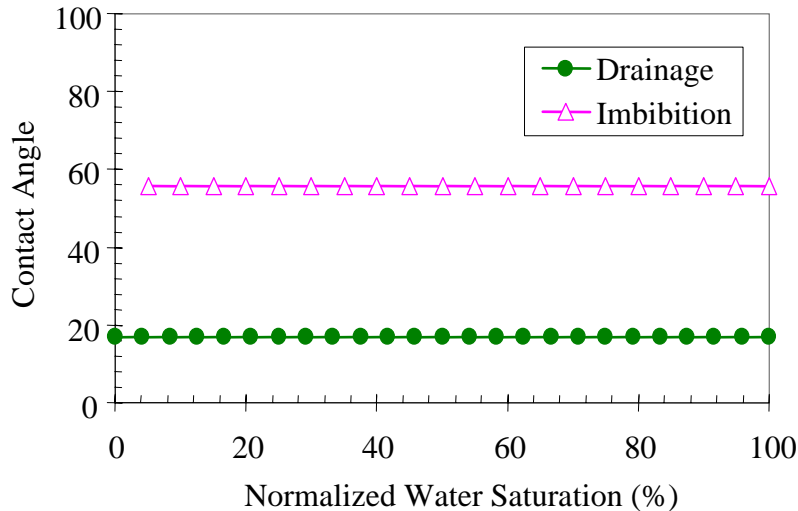


Figure 3.6: Contact angle calculated using data from Li and Horne (2000b).

The contact angle related to the drainage procession is usually referred to as the receding contact angle and that related to the imbibition procession as the advancing contact angle. As expected, Fig. 3.6 shows that the receding contact angle is smaller than the advancing contact angle.

Comparing the values of the wettability index in Fig. 3.5 to those in Fig. 3.2, we found that the wettability indices ($W_i=0.96$ for drainage and 0.56 for imbibition) in steam-water-rock systems are much greater than that ($W_i=0.12$) in oil-water-rock systems. This observation demonstrates that the method developed in this study to determine the wettability in steam-water-rock systems would be useful. An important feature of this method is that it is not only appropriate for liquid-liquid-rock systems but also for gas-liquid-rock systems.

3.6 CONCLUSIONS

Based on the present work, the following conclusions may be drawn:

1. A method was developed to determine the wettability in steam-water-rock systems using the data from experimental measurements of steam-water capillary pressure and relative permeability.
2. The method is appropriate to determine the wettability of the liquid-liquid-rock systems as well as the gas-liquid-rock systems.
3. It is possible to determine the wettability at any specific fluid saturation by using both capillary pressure and relative permeability data with the method developed in this study.

4. The wettability index calculated using the method developed here for the imbibition case is smaller than that for the drainage case, which has been proven experimentally.
5. The values of the wettability index in the gas-liquid-rock systems are greater than that in oil-water-rock systems, which is reasonable and consistent with previous observations.

3.7 FUTURE WORK

We will verify the method developed in this study using more data of capillary pressure and relative permeability.

4. FRACTURED ROCK RELATIVE PERMEABILITY

This project is being conducted by Research Assistant Mark D. Habana, Research Associate Kewen Li and Prof. Roland N. Horne. The objective is to measure relative permeability relations for steam and water flow in a fractured geothermal rock. This work is an extension of current studies of steam-water flows, which have so far considered only artificially uniform porous rock. In this stage of the project, nitrogen and helium were pumped into a fractured Geysers core to determine fracture effects. Also, tests were conducted of an electrical resistivity tomography (ERT) method for saturation measurement.

4.1 BACKGROUND

Various works on flow through fractures have shown different kinds of relative permeability behavior. Experimental studies by Persoff and Pruess (1995) reported curves that can not be classified either as Corey type or as linear (X-curve) type. Fourar et al. (1993) suggested that multiphase interaction in a fracture is a function of flow velocity and therefore relative permeability is not the appropriate way to describe multiphase flow in fractures.

Past experiments have used synthetic fabricated fractures and/or gas-water or oil-water as fluids. This experimental study will use a real fractured core from The Geysers geothermal field and steam and water as the flowing fluids.

Nitrogen and helium permeability experiments were conducted on the core to determine the effects of the rock fractures and to investigate the constraints and practicalities of conducting multiphase flow experiments in real geothermal rocks. The core contains several fractures as determined from an X-ray computer tomography image.

Experiments were also conducted to develop an electrical resistivity tomography (ERT) method to measure saturations in the core. This saturation measurement technique is a useful alternative to X-ray CT methods because of the long duration of the experiment and because of the need for high confining pressures in the planned steam-water relative permeability experiments.

4.2 EXPERIMENTAL METHODOLOGY

The rock permeability was measured using nitrogen and helium gas at room temperature. The apparatus used is shown in Figure 4.1. Since gas permeability is a function of pressure, as described by Equation 4.1, the flow measurements were conducted at a series of different mean pressures.

$$k_{gas} = k_{abs} \left(1 - \frac{b}{P_{ave}}\right) \quad (4.1)$$

The core sample was obtained from a depth of 1409.3m at The Geysers geothermal field. The piece used is 6.91 cm in length and 4.70 cm in diameter.

Nitrogen was flowed through the core in experiments at different confining pressures. Confining pressure from 500 to 850 psig was applied by injecting nitrogen around the heat shrink tubing inside the core holder. To apply a confining pressure of 1150 psig water was used in place of nitrogen.

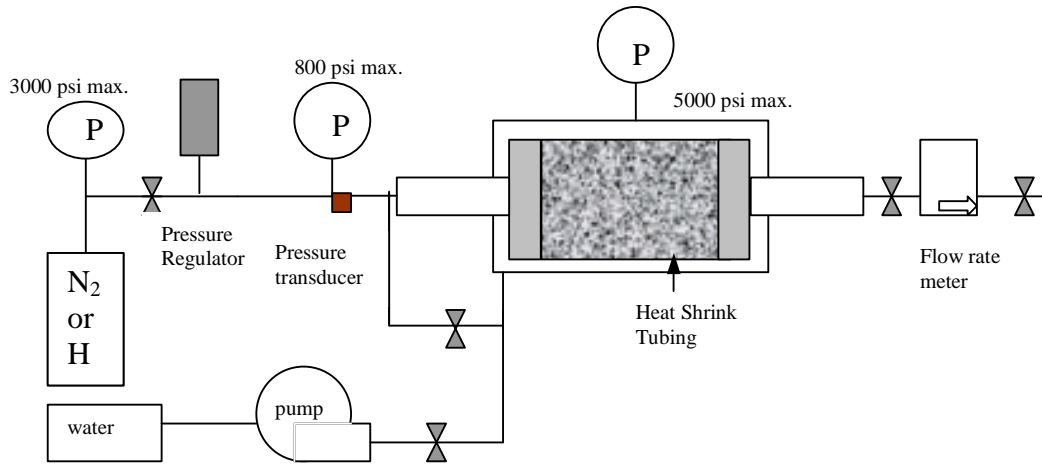


Figure 4.1: Apparatus for flow measurement in geothermal rock.

A pressure gauge and a pressure transducer connected to a digital display measured pressure at the inlet. The pressure at the outlet was taken to be 1 atm. The flow rate at the outlet was measured using a Matheson flow rate meter and controller (Model 8272-MF2000). The flow rate transducer calibration equation used was that determined by Kewen Li when he used the device in his experiments on slip factors (Oct-Dec 1999 Quarterly Report).

Two ERT experiments were done using a disc-shaped homogeneous rock. The same experiment was repeated using a heterogeneous rock. The apparatus is shown in Figure 4.2.

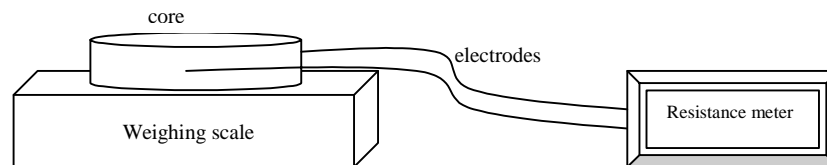


Figure 4.2: Apparatus for ERT experiments.

The core was saturated fully with water and then allowed to dry on a weighing scale. Electrical resistance was measured for every 1 gram decrease in mass of the saturated core. Resistivity and resistivity indices were calculated for each resistance reading by using Eqs. 4.2 and 4.3.

$$\rho = r \left(\frac{A}{L} \right) \tag{4.2}$$

$$R_{index} = \frac{\rho_{partiallysaturated}}{\rho_{fullysaturated}} \tag{4.3}$$

where r is resistance

A is area

L is length

ρ is resistivity

4.3 PARTIAL RESULTS AND DISCUSSION

Results of the nitrogen experiments are shown in Figure 4.3. The intersection of the extrapolated lines with the vertical axis in the plot of permeability (k) versus the reciprocal of the mean pressure ($1/p_{ave}$) is taken to be the absolute permeability of the rock. The values of permeability range between 0.58 to 1.2md.

It was observed that for the nitrogen experiments the permeability values decrease with increasing confining pressure. This can be attributed to the increase in net stress on the rock fractures as the confining pressure is increased. The increased net stress reduces the fracture aperture and, consequently, reduces the permeability.

There is a linear relationship between confining pressure and the absolute permeabilities obtained by extrapolation. This is shown in Figure 4.4.

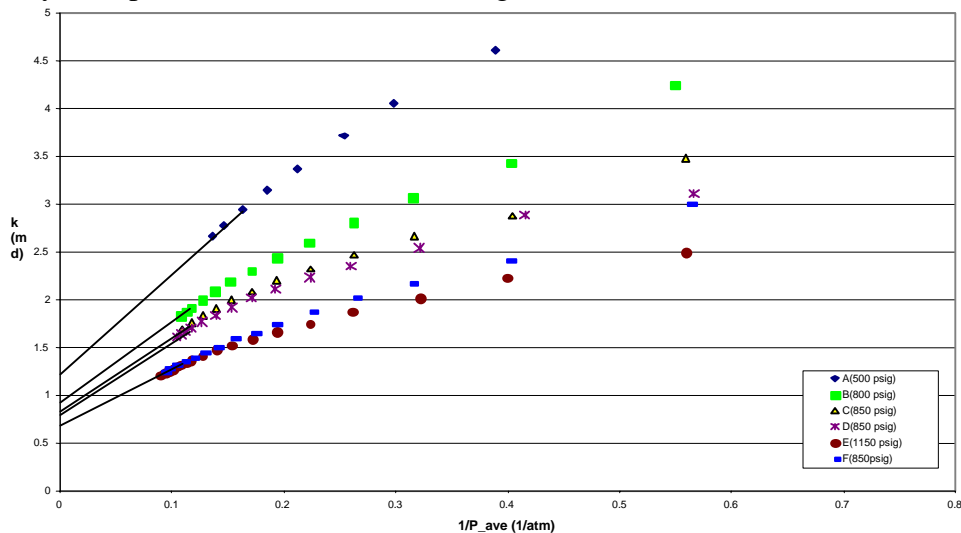


Figure 4.3: Results of nitrogen and helium permeability as a function of pressure.

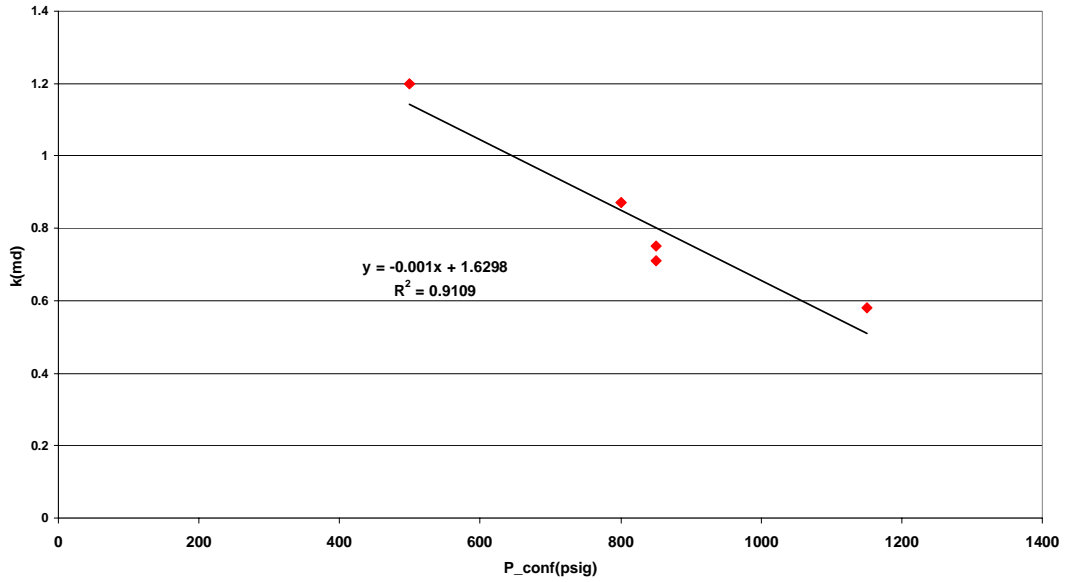


Figure 4.4: Absolute permeability results from nitrogen experiments.

Figures 4.5 and 4.6 show two helium experiment results compared to the two nitrogen experiments. All four flow experiments were at a confining pressure of 850 psig. For the helium experiment the permeabilities values obtained are higher than from the nitrogen experiments. Also, the slope for the helium experiment is lower than that for nitrogen at high confining pressures. This is not as expected. The slope for helium should be much steeper than that for nitrogen considering the difference in viscosities and molecular weights of the two fluids.

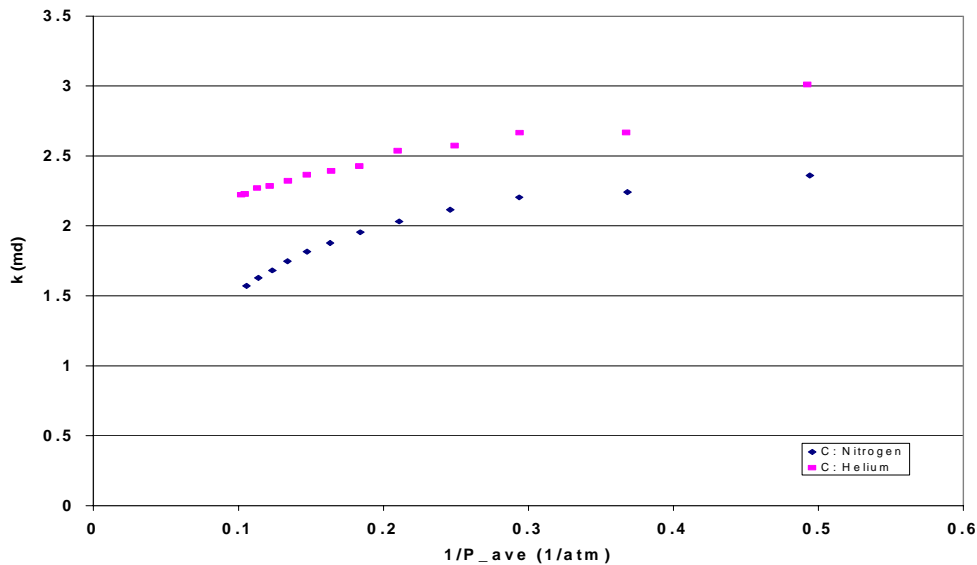


Figure 4.5: Results of helium and nitrogen permeability as a function of pressure.

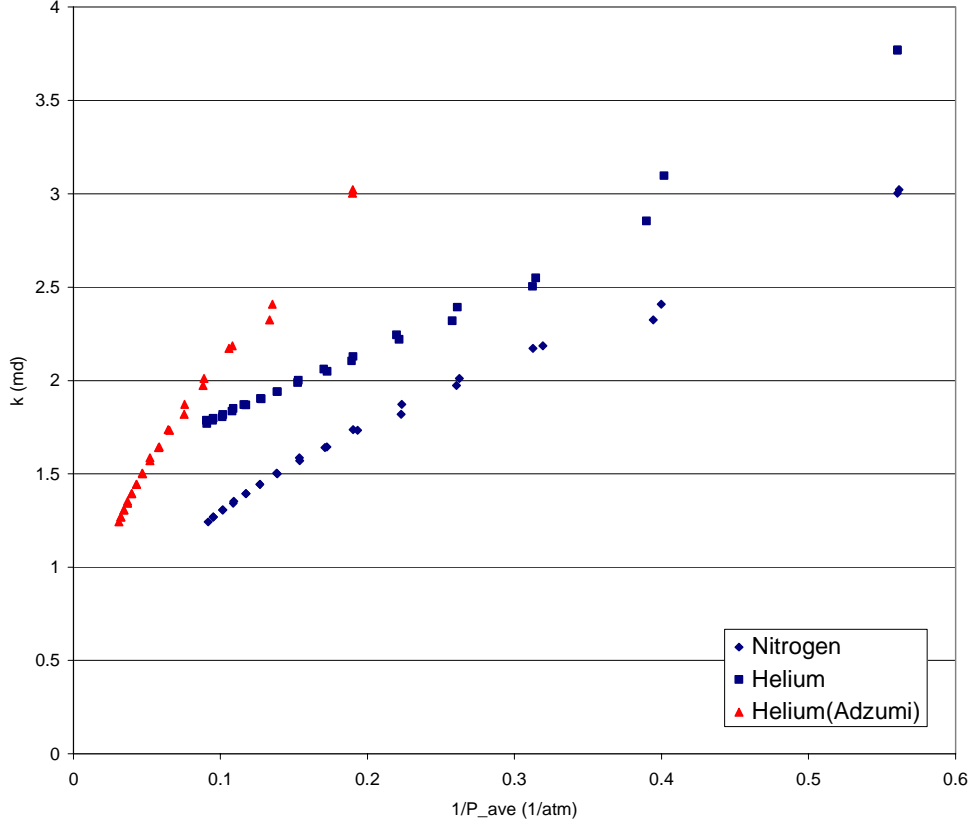


Figure 4.6: Calculated helium permeability values using Adzumi's equation and results of helium and nitrogen permeability as a function of pressure.

Assuming that the nitrogen data in Figure 4.6 is correct we can calculate the helium permeabilities for using Adzumi's equation, Equation 4.4.

$$\frac{p_2}{p_1} = \left(\frac{\mu_2}{\mu_1}\right) \sqrt{T_2 M_1 / T_1 M_2} \quad (4.4)$$

$$k_g(\text{gas 1 at } p_1 \text{ and } T_1) = k_g(\text{gas 2 at } p_2 \text{ and } T_2)$$

The calculated helium permeability values are shown as triangles in Figure 4.6. The permeability for a porous core is higher than that for a fractured core. This can be explained by a decrease or total closure of the aperture of the fractures due to the high net stress caused by the difference between the confining pressure and the pore pressure. Thus, at higher pore pressures the permeability values for the fractured medium may be greater than that for a porous medium.

The ERT experiment on the disc-shaped homogeneous rock showed a linear relationship between R_{index} and saturation in a log-log plot, Figure 4.7. This is very similar to the result obtained by Archie. For the heterogeneous rock, resistance readings were only obtained for a saturation range of 1 to 0.76, Figure 4.8. This is due to water drying out at the point of contact of the electrodes while most of the water is concentrated in the visible

fractures of the core. This is a challenge to the application of the ERT technique to saturation measurements in heterogeneous rocks.

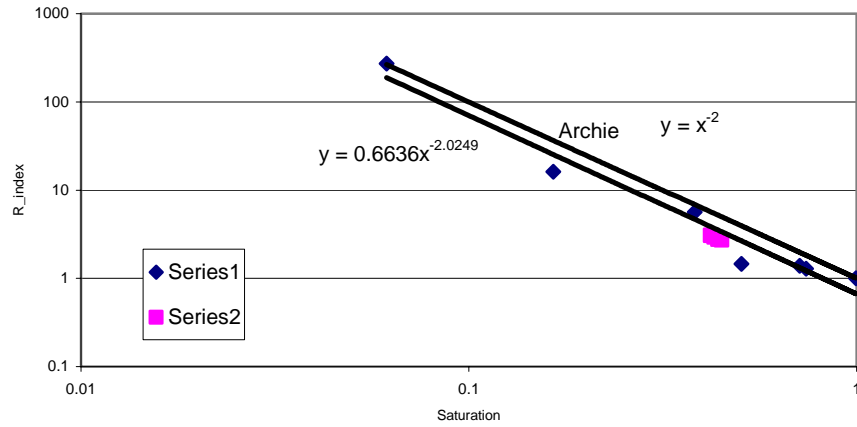


Figure 4.7: R_{index} versus water saturation for homogeneous rock.

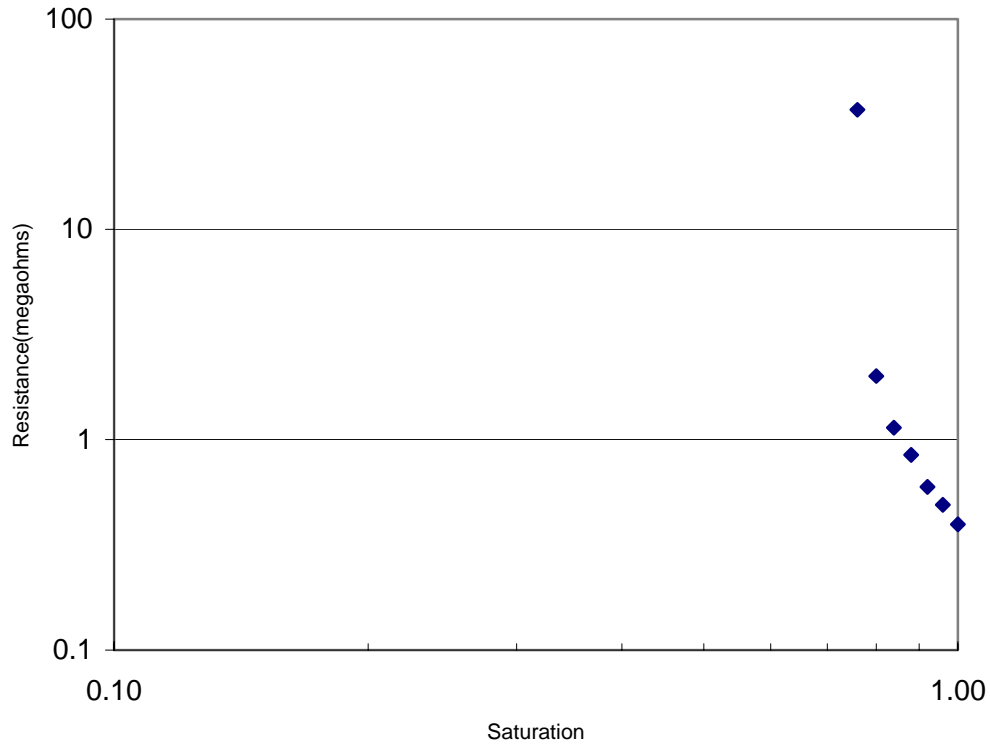


Figure 4.8: Resistance versus water saturation for heterogeneous rock.

4.4 CONTINUING AND FUTURE WORK

Design and construction of an ERT experiment to be conducted in the CT scanner is ongoing. This is being done to establish the effectiveness of the ERT method in determining saturations in the core by comparing with values obtained by the CT scanner.

After the water permeability experiment it is planned to do gas-water relative permeability experiments before proceeding to steam and water. The steam-water relative permeability experiment will be an unsteady state displacement process.

5. MEASUREMENT OF CAPILLARY PRESSURE IN GEOTHERMAL ROCKS

This research project is being conducted by Research Assistant Chih-Ying Chen, Research Associate Kewen Li, and Professor Roland Horne. The ultimate aim is to measure steam-water and air-water capillary pressures in fractured geothermal rocks. As a first step towards understanding the process, a simple experiment has been finished measuring capillary rise in narrow tubes. Preliminary data was acquired and will be used for future reference. A new capillary pressure experiment is being developed now. These experiments will attempt to measure both air-water and steam-water capillary pressure. An electrical resistivity measurement technique is being developed as an alternate way to infer capillary pressure.

5.1 BACKGROUND

Capillary pressure, an important but hard-to-measure physical property, plays a dominant role in reservoir performance and production forecasting. In the geothermal engineering field, the knowledge of the steam-water capillary pressure is limited because of difficulties in the measurement. Most of the difficulties come from the special relationship between the steam and the water phases. There is mass transfer between the steam and the water phase which makes conventional methods invalid or inaccurate. Horne et al. (1995) summarized the adsorption mechanism in geothermal reservoirs and described how adsorption curves could be used to infer capillary pressures. Sta. Maria and Pingol (1996), and Persoff and Hulen (1996) inferred values of steam-water capillary pressure from the adsorption data of Horne et al. (1995), and found steam-water capillary pressures ranging from 0 to 586 MPa (at 120°C) and 0 to 190 MPa (at 28.5°C) respectively. The difference between these two results is large. Li and Horne (2000c) developed a mathematical model to calculate steam-water capillary pressure of geothermal rocks using the steady-state steam-water flow experiment, and the results obtained were consistent with those measured by Persoff and Hulen (1996).

A capillary rise experiment is a straightforward way to measure the capillary pressure. A schematic of the capillary rise is shown in Figure 5.1. The capillary pressure can be obtained by using following equation:

$$P_c = \Delta\rho gh \quad (5.1)$$

where, $\Delta\rho = \rho_w - \rho_g$ denotes the difference in density between water phase and gas phase; g is the gravity constant and h is the height of the capillary rise to the meniscus above a flat liquid surface. The density of water is 0.9982 g/cm³ (at 20°C, 101 kPa), whereas the densities of air and steam is 0.0014 g/cm³ (at 20°C, 101 kPa) and 0.0000074 g/cm³ (at 20°C, 1 kPa), respectively. The density difference between air-water and steam-water systems seems very small. We should consider whether the difference between air-water and steam-water capillary pressure is significant or not. If the capillary pressure difference is not significant, air-water capillary pressure values could be used as a substitute for the steam-water capillary pressure. However, if the difference is significant,

it is necessary to develop a more accurate and efficient method to measure the steam-water capillary pressure.

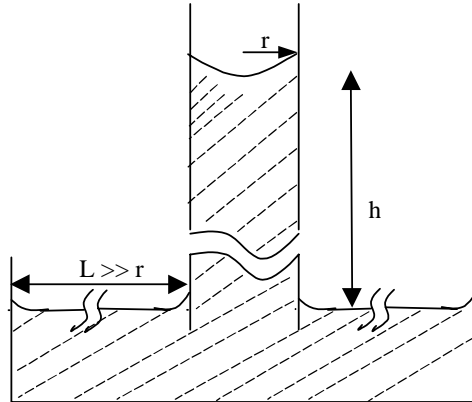


Figure 5.1: Capillary rise phenomenon (not to scale).

5.2 PRELIMINARY EXPERIMENTS

In the first stage, a capillary rise experiment was implemented to test whether any difference between air-water and steam-water capillary pressures can be distinguished. The apparatus is shown in Figure 5.2. The concept of this experiment is based on the capillary rise phenomenon (see Figure 5.1). The five capillary tubes used were Fisher 5 microliter borosilicate glass pipettes (Cat. No. 21-764-2B, TC $\pm 0.5\%$ accuracy) with average diameter 0.027cm, and length 12.7cm. Two plastic rulers with accuracy 1mm were used to measure the height of the capillary rise and water table. All of the tubes and rulers were adjusted to the same readings at the same height and were fixed to an aluminum bar which bridged the beaker horizontally. A vacuum pump (Welch Technology, Inc., Model 8915) was used to remove the air inside the chamber when the air inside the chamber measuring the steam-water capillary pressure (see Figure 5.2). A pressure transducer was installed to monitor the vacuum state and measure the pressure in the chamber.

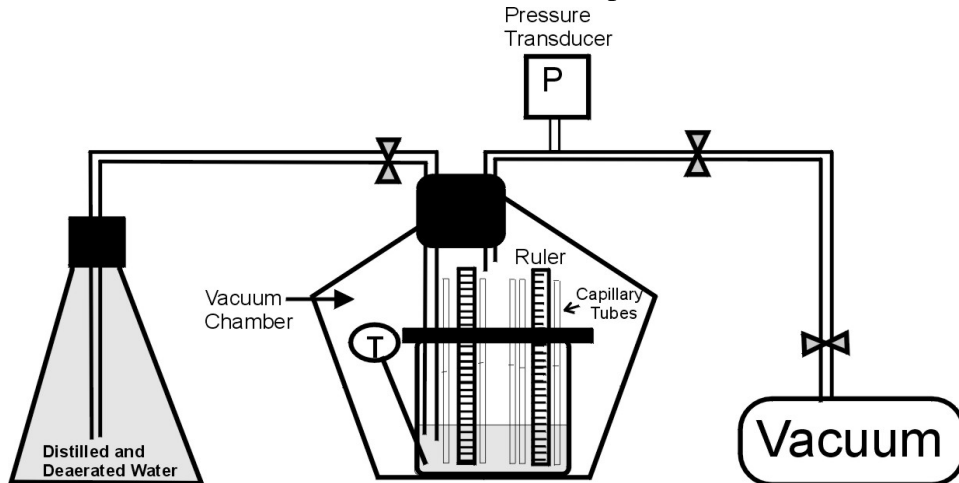


Figure 5.2: Schematic of apparatus of measuring steam-water and air-water capillary pressure.

The measured air-water and steam-water capillary pressures are shown in Table 5.1. The average air-water capillary pressure measured in this experiment was 31.6mm, and the average steam-water capillary pressure was 30.76mm. Only a slight difference between air-water and steam-water capillary pressure was found in this experiment. As can be seen in Table 5.1, the air-water capillary pressure measured in each tube is higher than the steam-water capillary pressure measured in the same tube. Air-water capillary pressure is higher on average than steam water capillary pressure by 0.84mm. Tube 2, tube 4, and tube 5 had the largest difference (1.0mm), whereas tube 1 had only a small difference (0.5mm). However it is not clear from these measurements whether these differences were attributable to differences between the air-water and steam-water capillary pressure. This is because some problems were found during this experiment when measuring the capillary pressure. The problems are attributed to: (a) the capillary balance time; (b) the hysteresis between imbibition and drainage; (c) the quality of the tubes, which were discussed in the previous quarterly report. According to Table 5.1, the difference between air-water and steam-water capillary pressure is near the ruler's minimum tick (1mm) and our visual measurement limit (0.5mm). Furthermore, the capillary pressure in different tubes ranged from 27mm to 34mm. This may be because the tubes were not uniform or each part of one tube has slight radius change. A skeptical attitude is still held at this preliminary stage.

Table 5.1: Measured air-water and steam-water capillary pressures.

	T (°C)	Pressure (psi)	Water Table (mm)	Tube 1 reading	Tube 1 Capillary Pressure	Tube 2 reading	Tube 2 Capillary Pressure	Tube 3 reading	Tube 3 Capillary Pressure	Tube 4 reading	Tube 4 Capillary Pressure	Tube 5 reading	Tube 5 Capillary Pressure
Air-water Experiment	22	14.7	31.5	61	29.5	63.5	32	65	33.5	66.5	35	59.5	28
Steam-water Experiment	22	~0	32	61	29	63	31	64.8	32.8	66	34	59	27
Capillary Pressure Difference					0.5		1		0.7		1		1

- *pressure unit is mm H₂O*

5.3 NEW EXPERIMENT

A more practical and applicable experiment has been designed using a real rock. A schematic of the new experiment is shown in Figures 5.3 and 5.4. This apparatus will be used to measure the air-water and steam-water capillary pressure of ceramic and Berea sandstone core samples with different water saturation. The properties of the samples are shown in Table 5.2. Two different types of cores will be used. The ceramic core sample has characteristics of high porosity and low permeability whereas the Berea sandstone has a low porosity and high permeability. The capillary pressure in different rocks can be represented using the J-function suggested by Leverett (1941) as follows:

$$P_c = \frac{\sigma \cos \theta}{\sqrt{\frac{k}{\phi}}} J(S_w) \quad (5.2)$$

where, σ , k , ϕ , S_w , and $J(S_w)$ are surface tension, permeability, porosity, water saturation and J-function, respectively. According to Eq. 5.2, the ceramic core sample must have much higher capillary pressure than the Berea sandstone sample because of its high porosity and low permeability properties. We plan to use this apparatus to measure both imbibition and drainage air-water and steam-water capillary pressures.

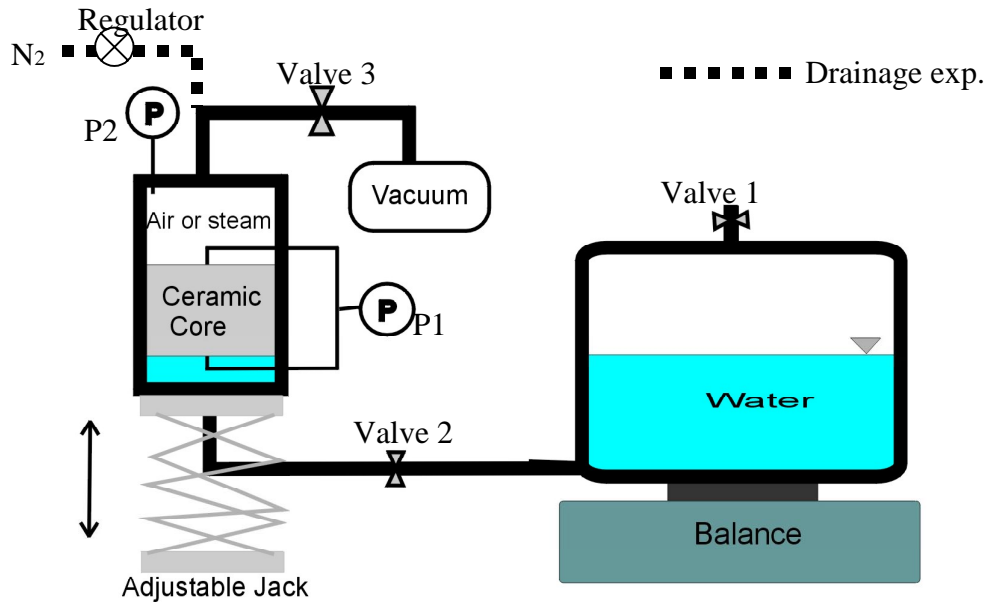


Figure 5.3: Schematic for the experiment of the air-water and steam-water capillary pressures in the ceramic core sample.

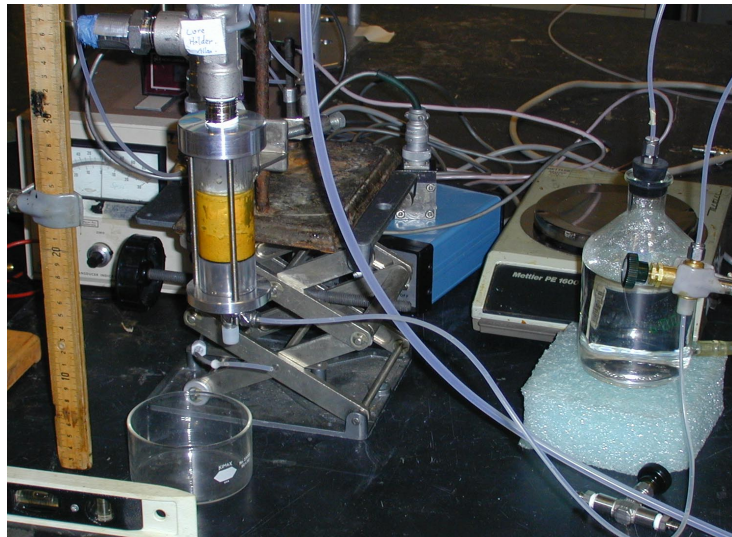


Figure 5.4: The apparatus of the air-water and steam-water capillary pressures experiment.

Table 5.2: Properties of samples studied.

Sample	Size (mm)	Pore Volume (ml)	Porosity (%)	Permeability (md)
Ceramic Core	25.62 D X 51.20 L	14.07	53.3	31.6
Berea Sandstone	25.68 D X 51.03 L	5.55	21	510

Procedure. In the imbibition experiment, water is imbibed into the core by opening Valve 2. The pressure difference between the top and bottom of the core sample can be measured in the pressure transducer P1, and the saturation can be measured by recording the reading change in the balance. In order to adjust the water saturation, an adjustable jack is used to lower the core holder vertically allowing more water to imbibe into the sample. For the steam-water capillary pressure, a vacuum pump is connected to the top of the core holder. Before injecting water inside the core sample, a certain amount of water is injected to the bottom of the core holder, and then vacuuming the core holder produces a steam environment. After that, water is injected to the core sample by opening Valve 2. The pressure difference between the top and bottom of the core sample, and the readings in the balance are recorded.

In the drainage experiment, for air-water capillary pressure, the core sample is fully saturated with water first. After saturation, the wet weight, W_{wet} is obtained by weighing the core holder. Then, nitrogen is injected into the core holder. A regulator is used to adjust the inlet nitrogen pressure. We start from a low inlet pressure and gradually increase it until there is a change in the balance reading. At this point, we define the entry capillary pressure. At this time, the saturation can be calculated using the following equation:

$$S_w = \frac{W_{i+1} - W_i}{W_{wet} - W_{dry}} \quad (5.3)$$

where, W_{wet} and W_{dry} denote the wet weight and dry weight of the core holder, respectively; W_i is the initial balance reading before flowing nitrogen inside the core holder; W_{i+1} is the reading recorded during nitrogen injection. The pressure can be measured by the pressure transducer P2. The pressure measured is the drainage capillary pressure of the sample. For the steam-water drainage capillary pressure, a corresponding method is still under development.

5.4 PARTIAL RESULT AND DISCUSSION

During the imbibition experiment, an unexpected gas bubble occurs between the bottom of the ceramic core sample and the water column. A schematic of this phenomenon is shown in Figure 5.5. This occurs because when the water saturation of the ceramic core is small, the capillary pressure is large enough to produce a vapor zone in the bottom of the

core sample. Once the gas bubble expands to the whole area of the cross section of the cold holder, the bubble will block the communication between water and the core. Hence, the pressure will recover due to this situation. Presently a new Berea sandstone core holder is being made. We plan to use the same method to measure the capillary pressure (drainage) of the Berea sample, to try to find a solution for the gas bubble problem.

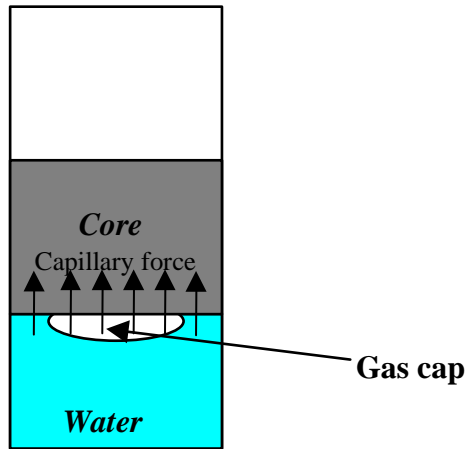


Figure 5.5: The formation of the gas bubble in the core holder.

The drainage experiment for the ceramic core sample is still being conducted. We estimate the entry pressure will be around 5 psi. A suitable pressure regulator has been configured and the stabilized test has been finished. The output pressure of the regulator can be maintained at a constant value with an accuracy of 0.0025 psi during the two-hour test time.

5.5 ELECTRICAL RESISTIVITY TOMOGRAPHY EXPERIMENT

The purpose of this experiment is to investigate the use of an indirect method to find the capillary pressure. The relationship between the electrical resistivity and water saturation can be represented by the following equation:

$$I = bS_w^{-n} \tag{5.3}$$

where, $I=R_t/R_o$, the resistivity index; R_t is the saturation measured; R_o is the resistivity of the rock when fully saturated with water; b is some function of tortuosity; and n is the saturation exponent. As we know, the capillary pressure is also function of the saturation. If a relationship between the resistivity and capillary pressure can be established, an easier resistivity measurement can be utilized to infer the corresponding capillary pressure, which is often more difficult to measure.

A preliminary Electrical Resistivity Tomography (ERT) test has been completed. The sample properties are shown in Table 5.3. The configuration of the electrodes is shown in Figure 5.6. Two sets of electrodes were installed in the hollow sandstone core, named the upper set and the lower set.

Table 5.3: Properties of samples tested.

Sample	Size (mm)	Pore Volume (ml)	Porosity (%)
Hollow sandstone core	49.78 OD X 31.87 ID X 51.20 L	15.3	26

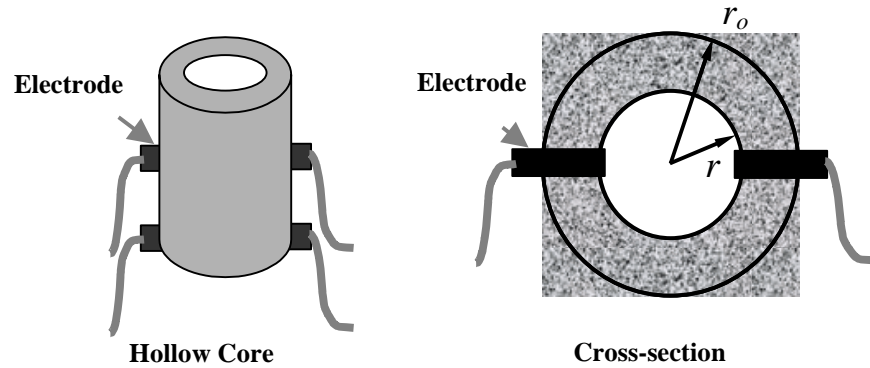


Figure 5.6: The installation of the electrodes in the hollow sandstone core.

The test result is shown in Figure 5.7. As can be seen, the resistivity curves are similar in shape to the drainage capillary curve. Also in Figure 5.7, because only the average saturation was measured during this test, the upper resistivity reading is different from the lower reading at the same average saturation value. A measurement of the saturation at the cross section where the electrode set is installed will be done in the next stage using the X-ray CT scanner or some other method. In the next stage a solid Berea sandstone core will be used. A comparison of the resistivity with the drainage capillary pressure measured using the semipermeable membrane method will be made.

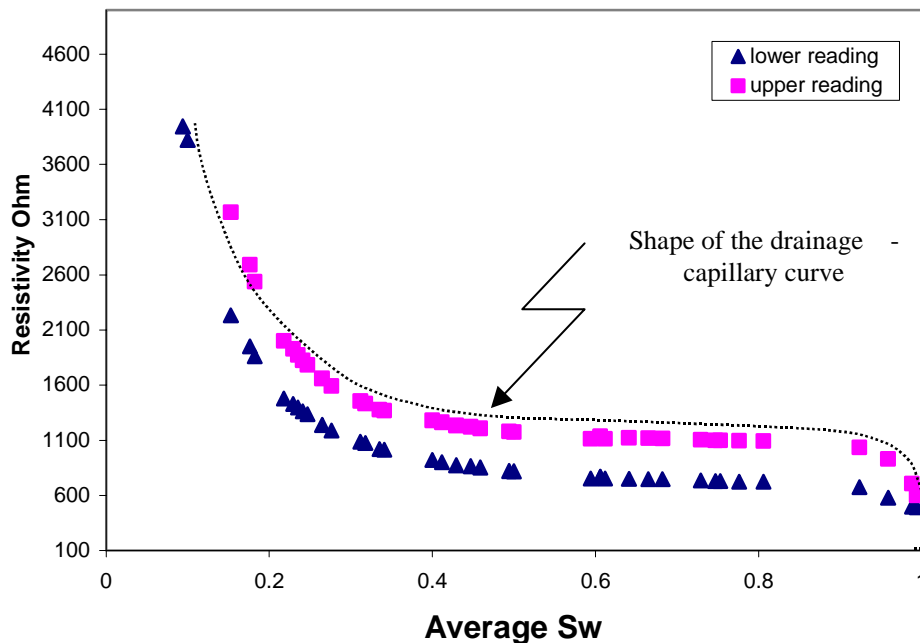


Figure 5.7: Measurements of resistivity in the hollow sandstone core.

5.6 FUTURE WORK

The result of the capillary rise experiment shows that air-water capillary pressure may be higher than steam-water capillary pressure by a small difference, but no definitive conclusion is possible at this stage. Now we are conducting the new experiment using both direct and indirect methods. Because of the failure of the ceramic core experiment (imbibition), modifications of the apparatus and procedure are needed. The ERT test shows a sensitive and consistent response when the saturation changes. This may be a useful way to infer the capillary pressure using the resistivity. A solid Berea sandstone core will be used in the next step. The result will be used to examine the feasibility of inferring the capillary pressure using the resistivity in different rocks, including actual geothermal cores.

Further research will also focus on the theoretical surface chemistry and thermodynamics governing air-water and steam-water capillary interfaces.

6. EXPERIMENTAL INVESTIGATION OF STEAM AND WATER RELATIVE PERMEABILITY ON SMOOTH WALLED FRACTURE

This project is being conducted by Research Assistant Gracel P. Diomampo, Research Associate Kewen Li and Prof. Roland Horne. The goal is to gain better understanding of steam-water flow through fractured media and determine the behavior of relative permeability in fractures.

6.1 BACKGROUND

Geothermal reservoirs are complex systems of porous and fractured rocks. Complete understanding of geothermal fluid flow requires knowledge of flow in both types of rocks. Several studies have been done to investigate steam and water flow through porous rocks but there is less understanding of multiphase flow in fractures. Only a few published data are available most of which have been done for air-water system or for water-oil systems. Earliest is the Romm (1966) experiment with kerosene and water through an artificial parallel-plate fracture lined with strips of polyethylene or waxed paper. Romm found a linear relationship between permeability and saturation, $S_w = k_{rw}$, $S_{nw} = k_{rnw}$ such that $k_{rw} + k_{rnw} = 1$. Pan et al. (1996) performed a similar experiment with an oil-water system but arrived at conflicting results. Significant phase interference was observed such that $k_{rw} + k_{rnw} < 1$. Both studies, however, concluded that residual saturations are zero such that a discontinuous phase can flow as discrete units (or “blobs”) along with the other phase.

In an attempt to develop a relationship between fracture relative permeability and void space geometry, Pruess and Tsang (1990) conducted numerical simulation for flow through rough-walled fractures. Their study shows the sum of the relative permeabilities is less than 1, residual saturation of the nonwetting phase is large and phase interference is greatly dependent on the presence or absence of spatial correlation of aperture in the direction of flow. Persoff et al. (1991) did experiments on gas and water flow through rough-walled fractures using transparent casts of natural fractured rocks. The experiment showed strong phase interference similar to the flow in porous media. Data of Persoff (1991) and Persoff and Pruess (1995) for flow through rough-walled fractures are compared in Figure 6.1.

Presently, the mechanism of flow and the characteristic behavior of relative permeability in fractures are still undetermined. Issues such as whether a discontinuous phase can travel as discrete units carried along by another phase or will be trapped as residual saturation as in a porous medium are unresolved. The question of phase interference i.e. is the relative permeability curve against saturation an X-curve, Corey or some other function is still unanswered. The main objective of this study is to contribute to the resolution of these issues. Experiments on flow through smooth-walled fractures will be done first for air-water flow with the aim of establishing a reliable methodology for flow characterization and permeability calculation. Then these experiments will be done with a steam-water system; and with rough-walled fractures.

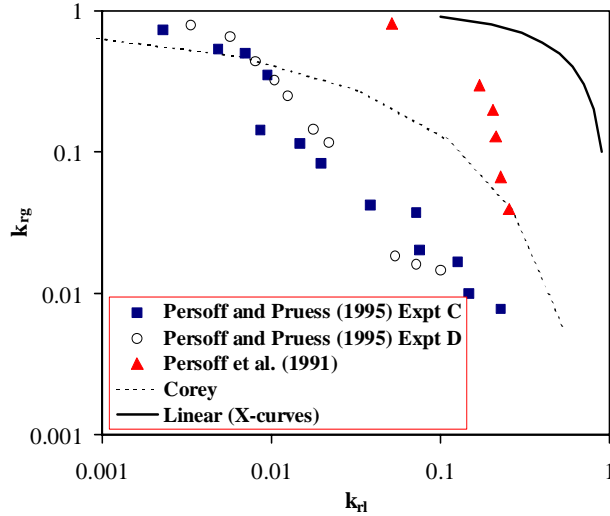


Figure 6.1: Some measurements of air-water relative permeabilities in rough-walled fractures (graph from Horne et al. 2000).

6.2 EXPERIMENTAL APPARATUS AND MEASUREMENT TECHNIQUES

The apparatus consists of a 183 cm. by 31 cm horizontal glass plate on top of an aluminum plate. The aperture is dictated by 0.2-mm thick shims inserted in between the glass and aluminum plates. The shims were placed along the boundaries and in three columns along the flow area. It should be noted that the shims placed as columns along the plate do not divide the plate into separate flow sections. This was deduced upon observing cross flow across the shims.

The sides of the plates are sealed together with a silicone adhesive. It was observed that even with the adhesive, the inlet head has to be kept below 15 cm to avoid leakage. Vacuum of 0-5 psi is pulled at the two-phase outlet. This creates greater pressure drop with out increasing the inlet head. Pulling a vacuum allows more flexibility with flow rate and helps prevent leakage.

Horizontal slits in the ends of the metal plate serve as entry and exit points for the fluids. There are two available canals for input of gas and liquid. The options to input nitrogen and water as separate streams or as mixed fluid in a single stream were tried. It was found that mixing the gas and water prior to input caused no significant improvement in fluid distribution. Thus, the gas and water streams were injected separately for simplicity, ease of flow rate control and inlet pressure reading.

Gas flow was controlled through a flow regulator. A meter pump controls the rate of liquid injection. Dye was dissolved in the injection reservoir for better phase identification. Figure 6.2 is a schematic diagram of this configuration.

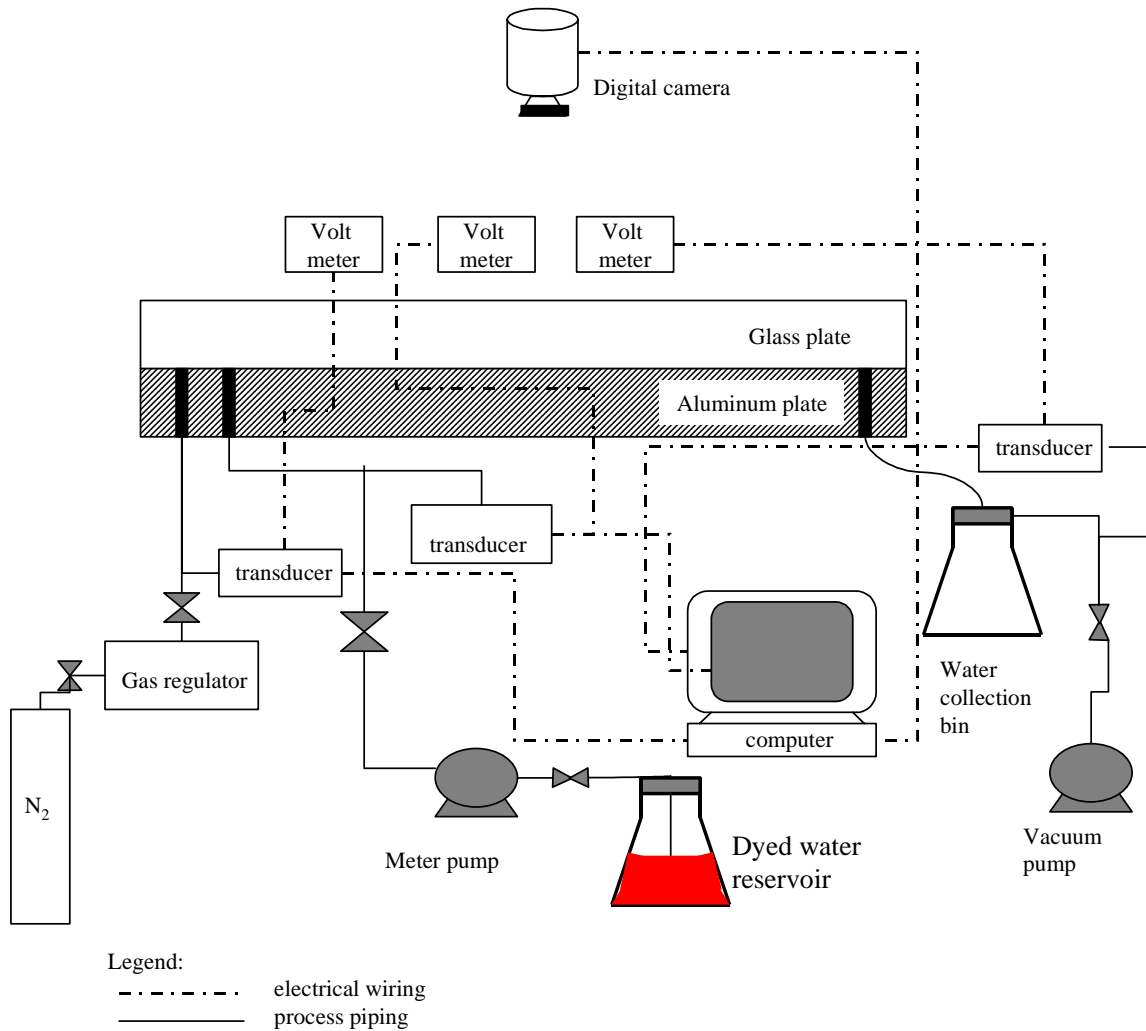


Figure 6.2: Apparatus for air and water flow through smooth walled fractures.

Water rate is read from the pump meter and gas rate from the regulator. Low range transducers measure the gas, liquid inlet pressure and the two-phase outlet pressure separately. These transducers are attached to a Labview program designed to record data at user-specified time intervals. Attached to each transducer is a voltmeter. The reading of the voltmeters is recorded with the two-phase flow image by the video camera. This is to gather the instantaneous pressure and saturation data simultaneously.

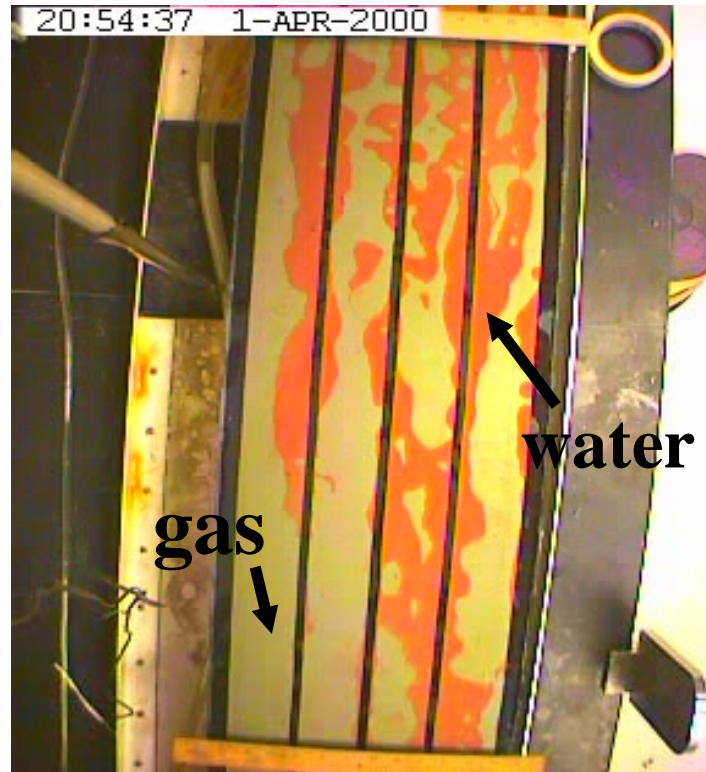
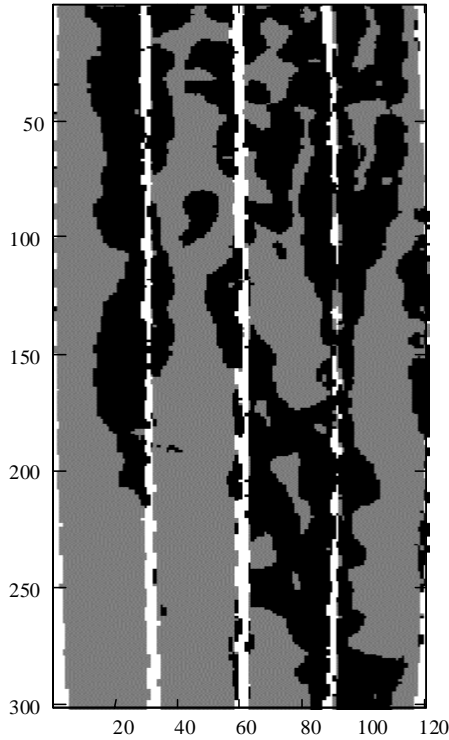


Figure 6.3: Sample camera image for two-phase run.

Saturation was computed by measuring the area that each phase occupied. This was done by taking digital images of a constant area of the plate at a particular gas and water rate. The area is around 3 ft. long, chosen far enough from the ends of the plates to prevent end effects. Figure 6.3 shows a sample image of a two-phase run. The photographs were processed in a Matlab program. The program uses quadratic discriminant analysis to group the pixels of the image into three groups: the water phase, gas phase and the shim. The grouping was based on color differences. Saturation was calculated as total pixels of liquid group over the sum of the gas and liquid group. Figure 6.4 shows a comparison of the gray scaled image produce by the program and the original photograph from the digital camera. The accuracy of the program in calculating the saturation can be related to the similarity in details of the gray scale image to the true image. From the figure, it can be said that the program has reasonable accuracy.



Saturation = 0.5987

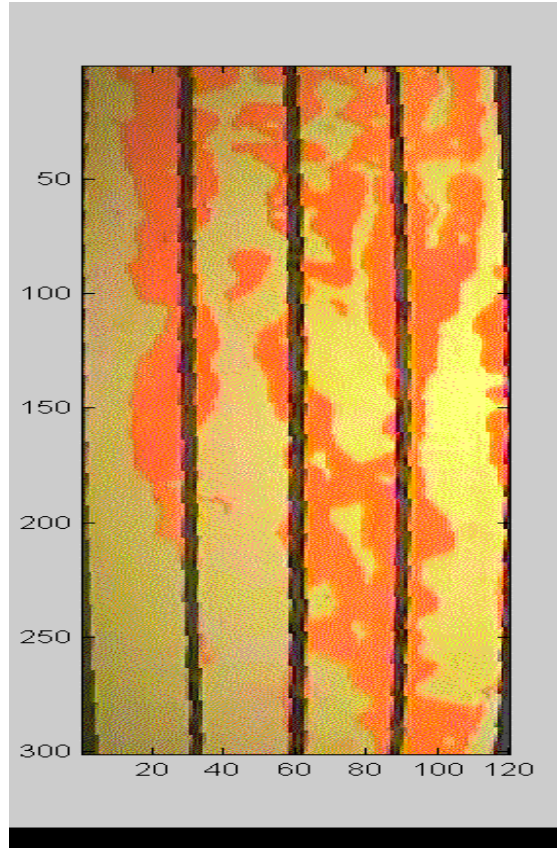


Figure 6.4: Comparison of gray image produced by Matlab program to actual photo taken by digital camera.

Pan et al. (1996) also used this technique for measurement of saturation. This study noted that the sources of error in this technique were the quality of the photographs and the water film adsorbed on the surfaces of the plates with the latter being of minimal effect. Good quality photographs are the ones with clear distinction between the gas and liquid phases. The use of dyed liquid enhanced visualization of phase boundaries and produced photographs of sufficient quality.

6.3 PARTIAL RESULTS AND DISCUSSION

Preliminary experiments were done with q_{gas}/q_{liq} values of 1, 5, 10, 20 and single-phase runs at residual saturation. There were some important observations:

At these ratios of q_{gas}/q_{liq} , the water and gas phase travel along the plate as separate channels. These separate flow paths change with time. This is illustrated in the series of images in Figure 6.5, which were taken at constant gas and liquid rate. This observation implies that at these ratios, the phases move individually and not as “moving islands” or “globules” of the discontinuous phase carried along by the other phase. It also suggests that there is no local steady-state saturation.

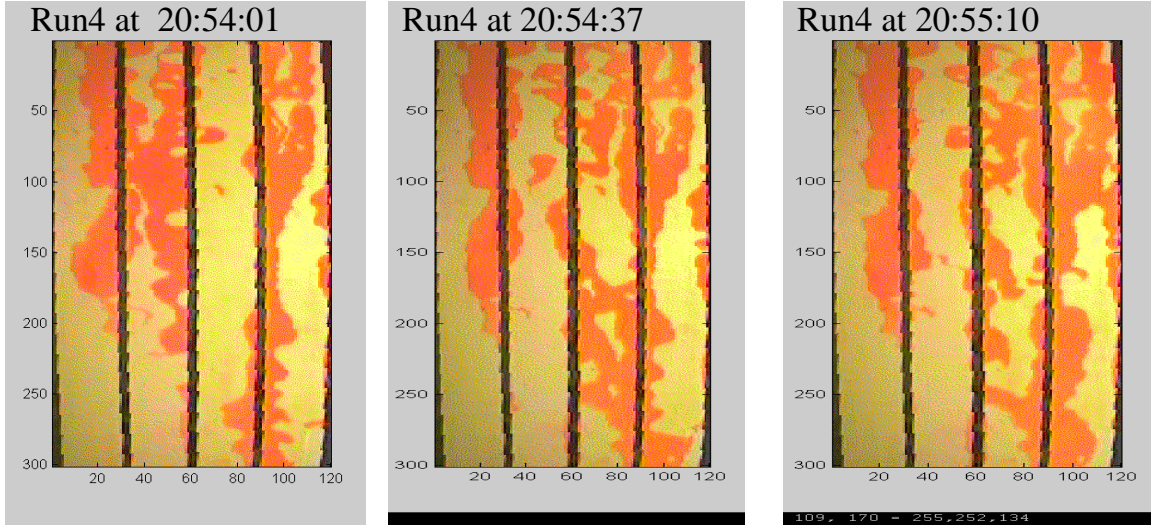


Figure 6.5: Images at constant gas and liquid rate in short time intervals to illustrate changes in the gas and liquid flow paths.

These fast changes in flow paths were accompanied by pressure fluctuations. When the gas had established enough energy to break through the water flow path, there was a corresponding increase in inlet gas pressure and decrease in water line pressure. The same was true when the water phase breached through gas channels. This caused difficulty in observing the pressure and was the reason why the pressure gauge readings were placed within the view of the video image in later experiments.

Residual saturations obtained were very low. S_{wr} was around 0.02 -0.06. Similarly, S_{gr} was around 0.04-0.06. This indicates that there was negligible trapping in this smooth-walled fracture.

Pan et al. (1996) discussed two approaches for data analysis: the porous medium approach where Darcy's law is used and the homogeneous single-phase approach where the system is treated as a single-phase pipe flow. Because of the observations in the experiments, it seemed appropriate to treat the data using porous medium approach.

Darcy's law was used to obtain the single-phase and two-phase liquid permeability:

$$k_l = \frac{q_i \mu L}{(p_i - p_o)} \quad (6.1)$$

subscript 'o' stands for outlet and 'i' for inlet, μ is the viscosity, p is pressure, L is length of the plate and q is the Darcy flow velocity from

$$q_o = \frac{Q_o}{bw} \quad (6.2)$$

where Q is the volumetric rate, b the aperture and w the width of the plate.

The relative permeability is then calculated by taking the ratio of the two-phase k_l with the single-phase k_l .

The gas permeability was calculated using the equation from Scheidegger (1974):

$$k_g = 2q_o\mu L \frac{p_o}{p_i^2 - p_o^2} \quad (6.3)$$

Similarly, taking the ratio of the two-phase k_g with single-phase run gives the relative permeability.

The complete list of calculated relative permeability values and their corresponding saturation range is shown in Table 6.1. Figures 6.6 and 6.7 show these data along with the X-curves. The data are clustered over a small saturation range and lie far from the X-curves.

Table 6.1: Calculated relative permeability values.

run #	Qg (cc/min)	Gas Head (cm H2O)	kr _g	Qw (cc/min)	Water Head (cm H2O)	kr _l
1	74	12.5	0.013	35.16	11.5	0.385
1	74	12.5	0.013	33.77	11.5	0.370
1	74	12.5	0.013	29.97	11.5	0.328
2	172	13	0.030	26.51	11.5	0.291
2	172	13	0.030	27.45	11.5	0.301
2	172	13	0.030	27.19	11.5	0.298
3	172	13	0.030	24.71	11.5	0.271
3	332	13.7	0.055	26.98	11.5	0.296
3	332	13.7	0.055	29.51	11.5	0.323
3	332	13.7	0.055	20.04	11.5	0.220
4	407	12.8	0.072	12.36	11.0	0.142
4	407	12.8	0.072	9.92	11.0	0.114
4	407	12.8	0.072	11.52	11.0	0.132

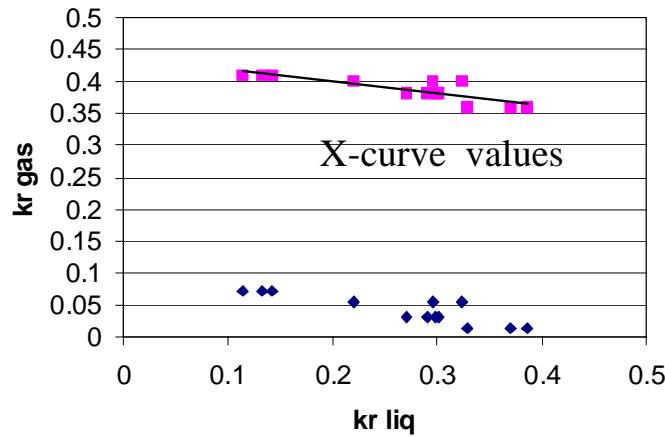


Figure 6.6: Comparison of experimental relative permeability values with X-curve values.

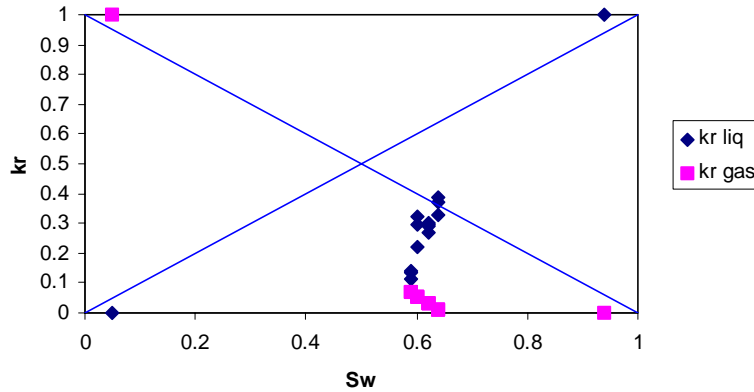


Figure 6.7: Experimental relative permeability values against saturation.

6.4 DESIGN OF STEAM-WATER APPARATUS

The general technique used in the design for steam water apparatus was to pattern it after the current nitrogen-water experiment. The issues faced in the design are gaining accurate measurement of steam, water inlet and outlet flow, instantaneous saturation and pressure measurement, confinement of high steam pressure, maintaining good isothermal conditions and prevention of leaks. With these many issues and uncertainty as to experimental results, the main steam-water fracture apparatus was designed in a way to be flexible to future changes.

The process flow diagram for the experiment is shown in Fig. 6.6. In this experiment, steam and water will be flowed separately into the fracture apparatus. The fracture apparatus will be kept at constant temperature. The two-phase outlet stream will be separated in a condenser.

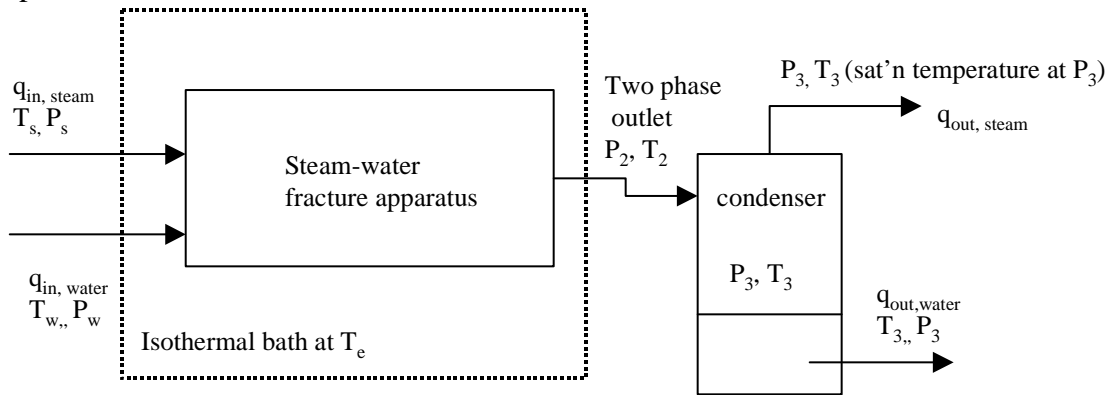


Figure 6.8: Process schematic for steam-water experiment.

Isothermal conditions will be maintained by putting the whole fracture apparatus in a constant temperature air bath. Mirrors will be placed in the oven to reflect the image of the flow towards a video camera. The video will be used to measure saturation and to study the flow mechanism.

The fracture apparatus is maintained as a glass plate on top of an aluminum plate. An o-ring is placed between the glass and aluminum plate as a seal. The whole apparatus is confined by another metal frame bolted to the bottom plate. This was done to improve the seal and to prevent deformation of the glass due to system pressure. The metal frame has a window for flow visualization (Figure 6.9).

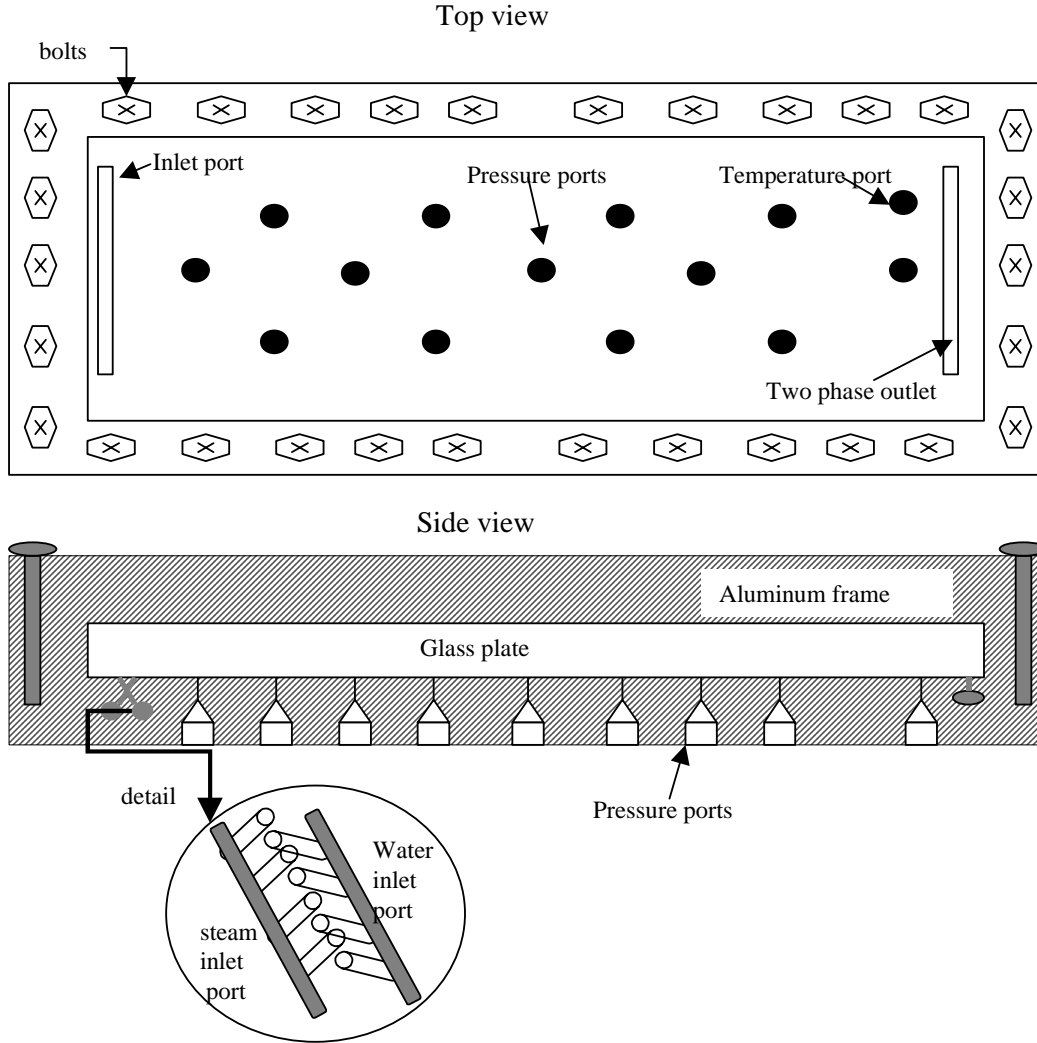


Figure 6.9: Schematic of steam-water fracture apparatus.

Steam and water enter to the fracture through two separate channels. Each channel has several ports drilled in a way that they align on the surface (Figure 6.9). Throughout the flow area, tiny pressure ports were drilled. Needle size ports were drilled so as to minimize surface discontinuity. One temperature port is drilled at one end.

The fracture apparatus was designed such that there is an available 12 inch by 4 inch space for flow. These dimensions were derived with the use of Equations 6.1 and 6.3. Given a set of relative permeability values, the equations were used to estimate pressure drop for different apparatus length and width. With the calculated pressure drop, an

estimate for the condensation rate of the steam and evaporation rate of the water phase is made. The dimensions were chosen so as to have minimum condensation, evaporation and system pressure.

The amount of steam that will condense through the apparatus is proportional to the heat lost. Heat lost (Q_{lost}) is due to the temperature difference between the entering steam (T_s) and surrounding temperature (T_e).

$$Q_{lost} = kA \frac{dT}{dx} \approx klw(T_s - T_e) / h \quad (6.4)$$

where k is the thermal conductivity of the glass, l , w and h are the length, width and height of the apparatus respectively.

The condensation rate is estimated by:

$$q_{condensation} = Q_{lost} / \Delta H_v \quad (6.5)$$

where ΔH_v is the latent heat of vaporization at T_s .

The amount of water that will vaporize is related to the drop in pressure as water flows from P_w to P_2 (refer to Figure 6.8). Energy balance gives:

$$x = \frac{(H_{sat'd_water_at_Pw} - H_{sat'd_water_at_P2})}{(H_{sat'd_vapor_at_P2} - H_{sat'd_water_at_P2})} \quad (6.6)$$

where x as weight fraction of steam, H represents enthalpy.

The glass plate is 1 inch thick. The thickness of the glass plate was calculated through Equation 6.7. This is to have a conservative estimate for minimizing buckling or glass deformation.

$$\Delta y_{max} = \frac{wl^4}{384EI} \quad (6.7)$$

where Δy_{max} represents the deformation of the glass vertically, E is the modulus of elasticity of the glass and I as the second moment of inertia equal to

$$I = \frac{lh^3}{12} \quad (6.8)$$

The new apparatus is shown in Figure 6.10.



Figure 6.10: Steam-water fracture apparatus.

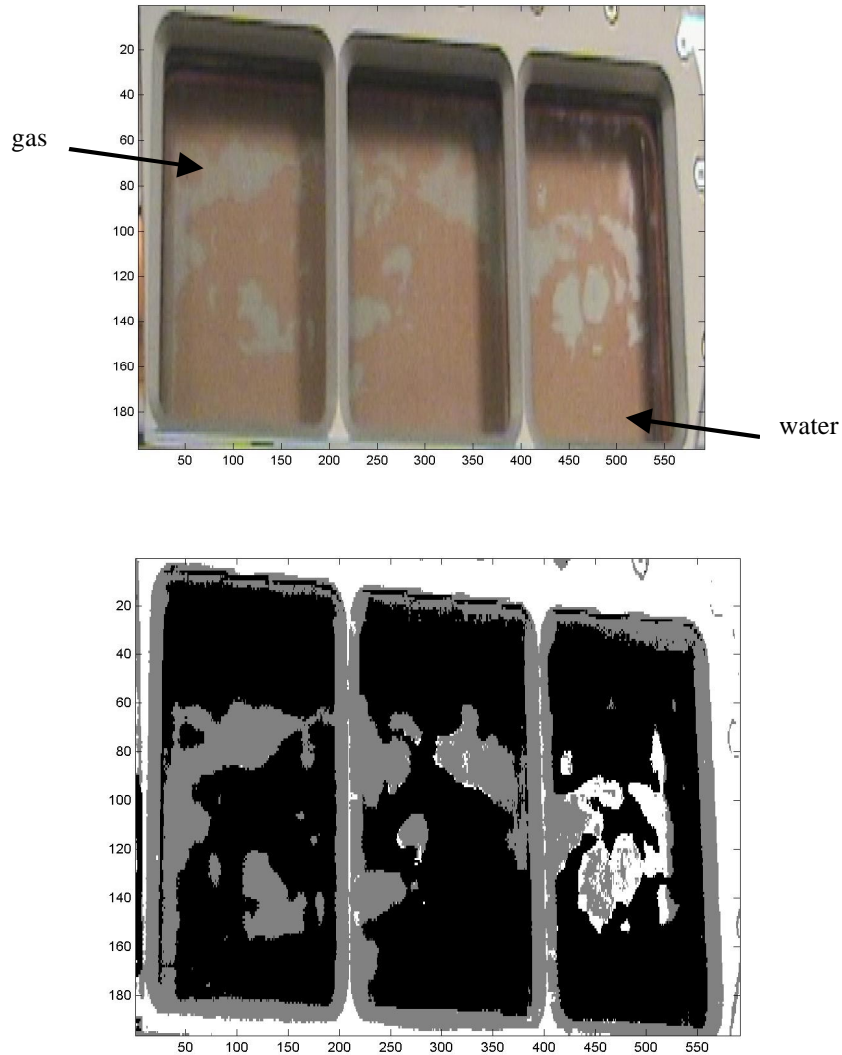
6.5 USE OF NEW APPARATUS FOR NITROGEN WATER EXPERIMENTS

There have been certain difficulties found in conducting the nitrogen-water experiments with the 183 by 31cm apparatus. Flow through the two inlet channels was not evenly distributed throughout the width of the apparatus. Water or gas will enter the apparatus only in selected chambers. To avoid this, a filter paper was inserted through the water inlet canal. This was effective in spreading the water evenly through the inlet portion. However, the water-saturated filter paper acted as an obstacle for the gas flow. The gas went through large pressure drops in order to flow through the filter paper. Regularly spaced openings were then cut through the filter paper in attempt to ease the gas entry. This inlet design is similar to the injection technique of Persoff and Pruess (1991). In their experiment, a slotted ceramic porous material was used as an inlet to facilitate flow distribution and also to prevent capillary end effects. In this experiment, however, the gas found it easier to flow at the ends of the channel width rather than at the filter paper openings. This resulted in gas flow being restricted to the extreme left and right chambers.

Given that flow was restricted only on certain chambers of the apparatus, the black shims separating the chambers were cut into pieces to facilitate pressure communication and mixing of the fluids. Mixing then occurred at the farther end, near the outlet. This requires that saturation and pressure data be taken at this location. However, there are no pressure ports in the intermediate locations of the apparatus. Another option would be to take the saturation of the whole length of the apparatus. Taking an image of the whole length of the apparatus sacrifices the image resolution. This would affect the accuracy of the saturation calculation. Also, capillary effects can be seen as water and gas flow through the gaps between chambers. With these difficulties, it was decided to use the new apparatus also for nitrogen-water experiments.

All the process piping from the previous apparatus was transferred to the new apparatus. The advantages the new apparatus are that it is relatively easier to seal, flow distribution is not a problem because the flow area is not be divided into chambers, input flow range

is not limited for it can withstand higher pressures and the aperture size can be easily changed. As a test run, water was injected at 8.5cc/min and gas at 1cc/min. Figure 6.11 shows the sample image run and the calculated saturation. In this image, it can be seen that the computer program was not able to differentiate to a high degree the gas phase and the metal casing. This can be due to the similarity in color of the silver metal casing and the gas phase. This implies that the program for saturation calculation or the lighting, color contrast of the elements in the apparatus need to be improved in order to achieve greater accuracy. This sample run however shows that nitrogen-water experiments can be done with greater ease and speed with the new apparatus.



Calculated Saturation = 0.7925

Figure 6.11: Comparison of flow image from the new apparatus and gray-scale image from Matlab program.

6.4 FUTURE WORK

Further experiments with nitrogen-water system will be done at higher order of variation of q_{gas}/q_{liq} . This is to obtain wider saturation range in the relative permeability values and to further investigate the flow mechanism. The experiment will also be done on system with sand or glass beads in between the glass and aluminum plate to simulate flow through rough walled fractures. Steam-water experiment with the new apparatus will also be conducted.

7. REFERENCES

- Anderson, A.W. and Gast, A.P.: "Physical Chemistry of Surface," 6th Edition, A Wiley-Interscience Publication, John Wiley & Sons, New York, 1997
- Brooks, R. H. and Corey, A. T.: "Properties of Porous Media Affecting Fluid Flow", *J. Irrig. Drain. Div.*, **6**, 61, 1966.
- Burdine, N. T.: "Relative Permeability Calculations from Pore Size Distribution Data", *Trans. AIME*, **198**, 71, 1953.
- Corey, A. T.: "The Interrelation between Gas and Oil Relative Permeabilities", *Prod. Mon.*, **19**, 38, 1954.
- Fatt, I. and Dykstra, H.: "Relative Permeability Studies", *Trans. AIME*, **192**, 249, 1951.
- Fourar, M., Bories, S., Lenormand, R., and Persoff, P.: Teo-phase Flow in Smooth and Rough Fractures: Measurement and Correlation by Porous Medium and Pipe Flow Models, *Water Resources Research* 29 (11), (1993), pp 3699-3708.
- Gates, J. I. and Leitz, W. J.: "Relative Permeabilities of California Cores by the Capillary Pressure Method", paper presented at the API meeting, Los Angeles, California, May 11, 1950, 286.
- Hanselman, D. and Littlefield, B. *Mastering Matlab 5 A Comprehensive Tutorial and Reference*, Prentice-Hall, Inc., New Jersey, 1998.
- Honarpour, M. M., Koederitz, L., and Harvey, A. H.: *Relative Permeability of Petroleum Reservoirs*, CRC press, 1986, ISBN 0-8493-5739-X.
- Horne, R.N., Ramey, H.J. Jr., Shang, S., Correa, A., and Hornbrook, J.: "The Effects of Adsorption and Desorption on Production and Reinjection in Vapor-Dominated Geothermal Fields," *Proc. of the World Geothermal Congress*, 1995, Florence, Italy, May, 1995, 1973-1977.
- Horne, R.N., Satik, C., Mahiya, G., Li, K., Ambusso, W., Tovar, R., Wang, C., and Nassori, H.: "Steam-Water Relative Permeability," presented at World Geothermal Congress, Kyushu-Tohoku, Japan, May 28-June 10, 2000; *GRC Trans. V. 24* (2000).
- Huang, D. D., Honarpour, M. M., Al-Hussainy, R.: "An Improved Model for Relative Permeability and Capillary Pressure Incorporating Wettability", SCA 9718, proceedings of International Symposium of the Society of Core Analysts, Calgary, Canada, September 7-10, 1997.
- Kleppe, J. and Morse, R. A.: "Oil Production from Fractured Reservoirs by Water Displacement," SPE 5084, presented at the 1974 SPE Annual Technical Conference and Exhibition, Houston, TX, USA, October 6-9, 1974.
- Land, C. S.: "Calculation of Imbibition Relative Permeability for Two- and Three-Phase Flow from Rock Properties", *SPEJ*, 149, June 1968.

- Land, C. S.: "Comparison of Calculated with Experimental Imbibition Relative Permeability", *Trans. AIME*, **251**, 419, 1971.
- Li, K. and Horne, R. N. (2000a): "Characterization of Spontaneous Water Imbibition into Gas-Saturated Rocks," SPE 62552, presented at the 2000 SPE/AAPG Western Regional Meeting, Long Beach, California, 19–23 June 2000
- Li, K. and Horne, R.N. (2000b): "Steam-Water Capillary Pressure," SPE 63224, presented at the 2000 SPE Annual Technical Conference and Exhibition, Dallas, TX, USA, October 1-4, 2000.
- Li, K. and Horne R.N. (2000c): "Steam-Water Capillary Pressure in Geothermal Systems," *Proc. of 25th Workshop on Geothermal Engineering*, Stanford, CA, Jan. 24-26, 2000.
- Li, K. and Horne, R.N.: (2001a) "Gas Slippage in Two-Phase Flow and the Effect of Temperature," SPE 5084, presented at the 1974 SPE Western Region Meeting, Bakersfield, CA, USA, March 26-30, 2001.
- Li, K. and Horne, R.N.: (2001b) "An Experimental Method of Measuring Steam-Water and Air-Water Capillary Pressures," paper 2001-84, presented at the Petroleum Society's Canadian International Petroleum Conference 2001, Calgary, Alberta, Canada, June 12–14, 2001.
- Li, K. and Horne R.N. (2001c): "Differences between Steam-Water and Air-Water Capillary Pressures," *Proc. of 26th Workshop on Geothermal Engineering*, Stanford, CA, Jan. 29-31, 2001.
- Mahiya, G.F.: *Experimental Measurement of Steam-Water Relative Permeability*, MS report, Stanford University, Stanford, Calif., 1999.
- Morrow, N.R. and McCaffery, F.G.: "Displacement Studies in Uniformly Wetted Porous Media," *Wetting, Spreading, and Adhesion, Academic Press*, New York, 1978, 289-319.
- Pan, X., Wong, R.C., and Maini, B.B.: Steady State Two-Phase Flow in a Smooth Parallel Fracture, presented at the 47th Annual Technical Meeting of the Petroleum Society in Calgary, Alberta, Canada, June 10-12, 1996.
- Persoff, P. and Hulen, J.B.: "Hydrologic Characterization of Four Cores from the Geysers Coring Project," *Proc. of 21st Workshop on Geothermal Engineering*, Stanford, CA, 1996.
- Persoff, P., and Pruess, K.: Two-Phase Flow Visualization and Relative Permeability Measurement in Transparent Replicas of Rough-Walled Fractures, *Proceedings, 16th Workshop on Geothermal Reservoir Engineering*, Stanford University, Stanford, CA, Jan. 23-25, 1991, pp 203-210.

- Persoff, P., and Pruess, K.: Two-Phase Flow Visualization and Relative Permeability Measurement in Natural Rough-Walled Fractures, *Water Resources Research* 31(5), (1995), pp 1175-1186.
- Persoff, P., Pruess, K., and Myer, L.: Two-Phase Flow Visualization and Relative Permeability Measurement in Transparent Replicas of Rough-Walled Fractures, *Proceedings, 16th Workshop on Geothermal Reservoir Engineering*, Stanford University, Stanford, CA, Jan, 23-25, 1991, pp 203-210.
- Pruess, K., and Tsang, Y. W.: On Two-Phase Relative Permeability and Capillary Pressure of Rough-Walled Rock Fractures, *Water Resources Research* 26 (9), (1990), pp 1915-1926.
- Purcell, W.R.: "Capillary Pressures-Their Measurement Using Mercury and the Calculation of Permeability", *Trans. AIME*, **186**, 39, 1949.
- Rapoport, L. A. and Leas, W. J.: "Relative Permeability to Liquid in Liquid - Gas System", *Trans. AIME*, **192**, 83, 1951.
- Romm, E. S: *Fluid Flow in Fractured Rocks*, Neda PUBLISHING House, Moscow, (English translation, Blackie, W.R., Bartlesville, OK, 1972).
- Scheidegger, A.E. *The Physics of Flow Through Porous Media*, 3rd ed., University of Toronto, Toronto. 1974.
- Sta. Maria, R.B. and Pingol, A.S.: "Simulation the Effects of Adsorption and Capillary Forces in Geothermal reservoirs," *Proc. of 21st Workshop on Geothermal Engineering*, Stanford, CA, 1996.
- Wyllie, M. R. and Gardner, G. H. F.: "The Generalized Kozeny-Carmen Equation, Its Application to Problems of Multi-Phase Flow in Porous Media", *World Oil*, **146**, 121, 1958.